M&P-0/127
For Author's Correction Only

Mineralogy and Petrology (2006) 00: 1–28
DOI 10.1007/s00710-006-0127-7

Mineralogy and Petrology

Printed in Austria

Tellurides, selenides and Bi-mineral assemblages from the Río Narcea Gold Belt, Asturias, Spain: genetic implications in Cu–Au and Au skarns

A. Cepedal[1], **M. Fuertes-Fuente**[1], **A. Martín-Izard**[1], **S. González-Nistal**[2], and **L. Rodríguez-Pevida**[2]

[1] Department of Geology, University of Oviedo, Spain
[2] Río Narcea Gold Mines

Received April 11, 2005; revised version accepted March 14, 2006
Published online • •, 2006;
Editorial handling: C. L. Ciobanu

Summary

Gold ores in skarns from the Río Narcea Gold Belt are associated with Bi–Te(–Se)-bearing minerals. These mineral assemblages have been used to compare two different skarns from this belt, a Cu–Au skarn (calcic and magnesian) from the El Valle deposit, and a Au-reduced calcic skarn from the Ortosa deposit. In the former, gold mineralization occurs associated with Cu–(Fe)-sulfides (chalcopyrite, bornite, chalcocite-digenite), commonly in the presence of magnetite. Gold occurs mainly as native gold and electrum. Au-tellurides (petzite, sylvanite, calaverite) are locally present; other tellurides are hessite, clausthalite and coloradoite. The Bi-bearing minerals related to gold are Bi-sulfosalts (wittichenite, emplectite, aikinite, bismuthinite), native bismuth, and Bi-tellurides and selenides (tetradymite, kawazulite, tsumoite). The speciation of Bi-tellurides with $Bi/Te(Se+S) \leq 1$, the presence of magnetite and the abundance of precious metal tellurides and clausthalite indicate fO_2 conditions with in the magnetite stability field that locally overlap the magnetite-hematite buffer. In Ortosa deposit, gold essentially occurs as native gold and maldonite and is commonly related to pyrrhotite and to the replacement of löllingite by arsenopyrite, indicating lower fO_2 conditions for gold mineralization than those for El Valle deposit. This fact is confirmed by the speciation of Bi-tellurides and selenides (hedleyite, joséite-B, joséite-A, ikunolite-laitakarite) with $Bi/Te(+Se+S) \geq 1$.

Introduction

Tellurides, selenides and Bi-sulfosalts are a group of minerals, in the following referred to as TSB, which are present as trace constituents in many types of gold

deposits, not only in skarn deposits, but also in porphyry-type and epithermal deposits (e.g. *Ciobanu* and *Cook*, 2002). These minerals can be valuable indicators of physicochemical conditions of formation in ore systems, because they are highly sensitive to changes in temperature and to fS_2 and fO_2 and pH conditions.

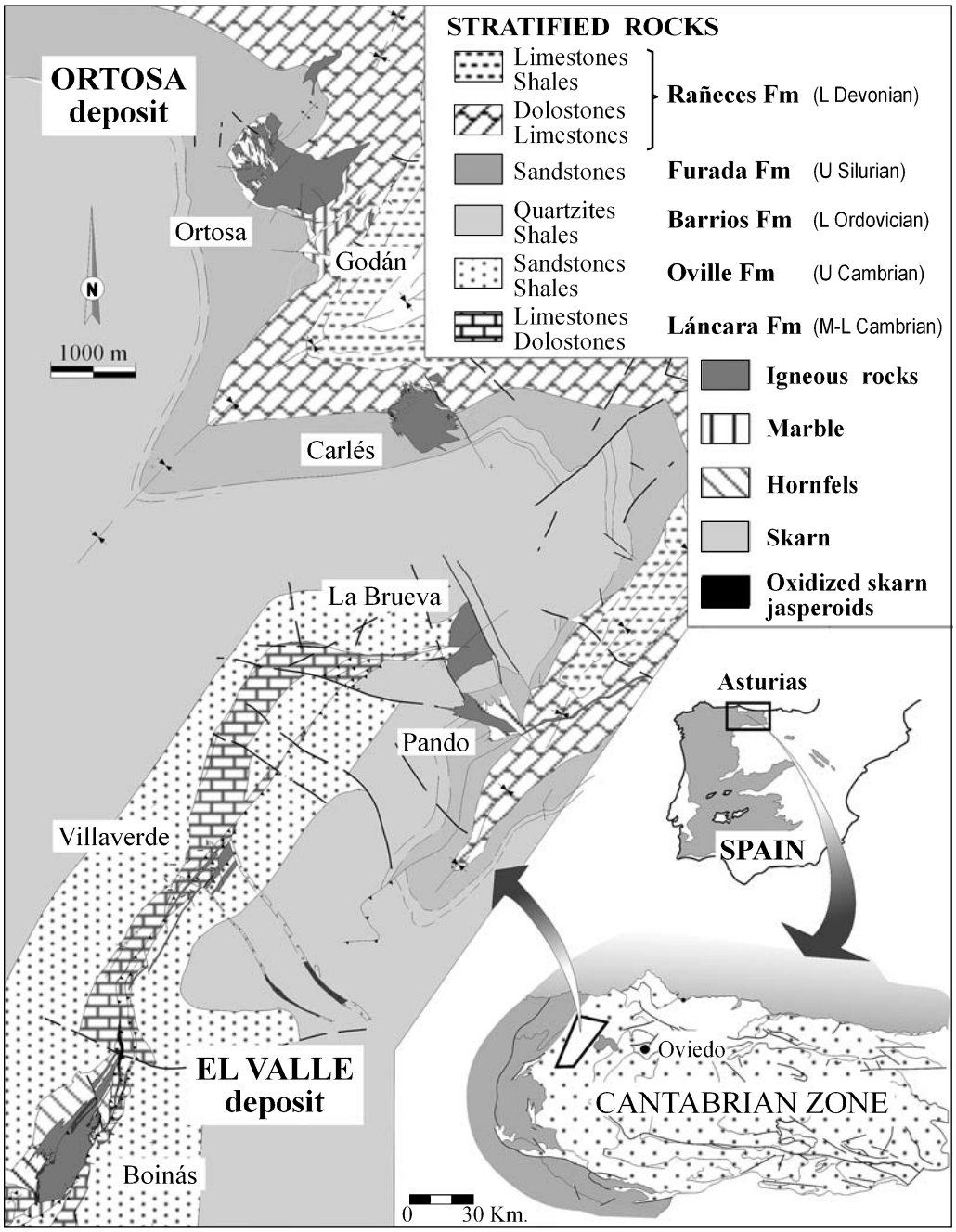

Fig. 1. Location and pre-Tertiary geological map of the Río Narcea Gold Belt (RNGB) skarns and igneous bodies (modified from *Martín-Izard* et al., 2000a)

The Río Narcea Gold Belt (RNGB) is one of four gold belts identified in the northwestern of the Iberian Peninsula (*Spiering* et al., 2000) and is currently the most important gold producer in Europe with two operating mines, El Valle and Carlés (Fig. 1). The Río Narcea gold operations produced more than of 911,000 oz of gold until September 2005, with an average grade of 6.0 g/t Au (*RNGM Website:* http://www.rionarcea.com). The El Valle mine started operations in the beginning of 1998. The company ceased open pit mining in 2004 and currently focuses on underground exploitation. Total mineral reserves at El Valle underground mine, estimated in December 2004, are 102,000 oz of gold at 5.7 g/t Au, and 7,140 t of copper at 1.10% Cu (*RNGM Website*: http://www.rionarcea.com). The Carlés open pit satellite mine started production, in the autumn 2000 and currently contributes around 10% of Río Narcea's annual gold production.

Deposits within the belt were formed by multiple gold-mineralizing events representing several styles of mineralization, including skarns, in a structurally complex, but favorable terrain of Paleozoic carbonate and siliciclastic host rocks. The two main skarn types developed in the RNGB are Cu–Au, calcic and magnesian, and Au-reduced calcic skarns. The El Valle and Carlés deposits are good examples of Cu–Au skarns, whereas the Ortosa deposit (Fig. 1) is a typical reduced Au skarn (*Fuertes-Fuente* et al., 2000). Despite its economic potential, the Ortosa deposit at present is, an exploration target only. Geochemical and petrographic observations show that gold mineralization is spatially associated with the occurrence of bismuth and tellurium giving rise to a large number of Au–Bi–Te–Se bearing minerals.

The presence of a number of TSB minerals in the skarns of the RNGM has been previously reported (*Arcos*, 1996; *Cepedal*, 2001; *Cepedal* et al., 2000, 2003; *Fuertes-Fuente* et al., 2000; *Martín-Izard* et al., 2000b). However, so far no studies have investigated the detailed, mineralogy or attempted to use it for constraining the physicochemical conditions of skarn formation. This paper comprises a comparative study of gold-related TSB minerals in two different skarns from the RNGB: the Cu–Au skarn from the El Valle deposit, and the Au-reduced skarn from the Ortosa deposit. The aims of this paper are to document the different mineral phases found in these deposits and to constrain the physical and chemical conditions during gold deposition.

Regional geology

The RNGB is located in the northern part of the Iberian Peninsula, within the Cantabrian Zone of the Iberian Variscan Massif, which represents the westernmost exposure of the European Variscides, where the largest exposure of pre-Permian rocks is located (Fig. 1). The Cantabrian Zone is characterized by a non-metamorphosed sedimentary succession, which includes a pre-orogenic pre-Carboniferous Palaeozoic sequence, with clastic and carbonate sediments, resting unconformably on a Precambrian basement. The Carboniferous units correspond to a syn-orogenic sequence that was principally clastic in the Upper Carboniferous. During the Variscan Orogeny, the Cantabrian Zone was thrusted, folded and faulted (*Pérez-Estaún* and *Bastida*, 1990). Several regional E–W, NE–SW and NW–SE fault systems dissect the unit. Among these, the most significant one for gold mineralization is an

NE–SW-oriented system, which has an extended history of reactivation. This system formed preferential sites for post-orogenic calc-alkaline igneous intrusions (*Jahoda* et al., 1989; *Corretgé* and *Suárez*, 1990; *Gutiérrez-Claverol* et al., 1991; *Spiering* et al., 2000; *Martín-Izard* et al., 2000a).

There are numerous I-type calc-alkaline granitoids (Fig. 1) and Au-bearing skarns related to these intrusions in the RNGB. The best known skarns are those related to the Boinás, Carlés and Ortosa intrusions (Fig. 1). Numerous previous studies have been undertaken (*Arcos*, 1996; *Arcos* et al., 1995; *Cepedal*, 2001; *Cepedal* et al., 2000, 2003; *Fuertes-Fuente* et al., 2000; *García Iglesias* and *Loredo*, 1990; *Martín-Izard* et al., 1993, 2000b). The Boinás intrusion produced calcic and magnesian Cu–Au skarns in Cambrian limestone and dolostone, respectively. The Carlés intrusion also produced a calcic Cu–Au skarn in Devonian limestones. The Ortosa intrusion developed Au-reduced calcic skarn in impure limestones at the top of a siliciclastic formation of Silurian age.

During Pre-Mesozoic extension, the belt was affected by reactivation of the previous structures and the intrusion of sub-volcanic dikes that produced hydrothermal alteration in several areas, rock brecciation and a low-temperature gold mineralization in argillized and silicified rocks (*Martín-Izard* et al., 2000a; *Fuertes-Fuente* et al., 2004). Moreover, thrust faults developed during Alpine deformation complicated the structure, producing new brecciation and remobilization of minerals. The basement is unconformably overlain by Tertiary sediments.

Skarn geology

This paper focuses on TSB mineral assemblages from the skarn ores of the El Valle and Ortosa deposits. In this section, we will give a summary of the petrographic and mineralogical characteristics of these two skarns, which have been more extensively described in *Cepedal* et al. (2000, 2003), *Cepedal* (2001) and *Fuertes-Fuente* et al. (2000).

The Boinás intrusion and the Cu–Au skarns of El Valle Deposit

The Boinás intrusive body actually consists of two different stocks (Fig. 2a). The younger is a porphyritic monzogranite, whereas the older ranges in composition from quartz-monzonite to monzogranite. The intrusion of these granitoids at 300 ± 5 Ma (*Martín-Izard* et al., 2000a) led to the formation of two different Cu–Au skarn types, calcic and magnesian in the Cambrian limestones and dolostones, in addition to endoskarn mineralization in the igneous rocks. Three mineralized areas are located around the intrusive body: Boinás West, Boinás East and El Valle (Fig. 2a). Magnesian and calcic skarns are found in El Valle and, particularly, in Boinás East. In Boinás West, only calcic skarn was developed.

The calcic skarn consists mostly of garnet (Adr_{20-100}), pyroxene (Hd_{3-97}), wollastonite, and lesser amounts of vesuvianite. Skarn zonation is expressed in terms of the mineralogy and changing chemical compositions of the main calc-silicate minerals. Proximal skarn consists of coarse-grained grossular garnet (Gr_{20-50}) and intermediate pyroxene (Hd_{28-52}); the pyroxene/garnet ratio increases towards distal parts of the skarn. Wollastonite and an early Fe-poor pyroxene (Hd_{3-28}) form

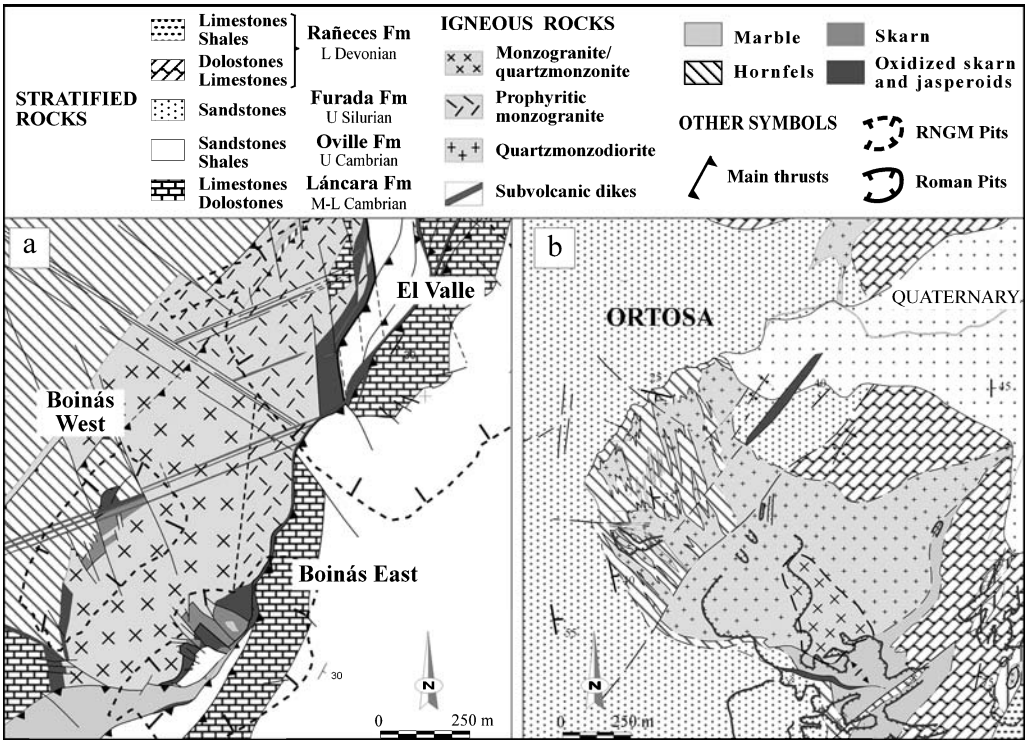

Fig. 2. **a** Geological map of the El Valle deposit. **b** Geological map of the Ortosa deposit. (Data provided by Río Narcea Gold Mines)

a banded skarn close to the contact with marble. Iron enrichment during skarn formation is indicated by the presence of andradite ($Adr_{70\approx100}$) and hedenbergite ($Hd_{70–97}$). This Fe-rich pyroxene continued to form during the first retrograde stage, which is characterized by epidote ($Ps_{22–27}$), amphibole ($Tr_{20–58}$), quartz, calcite, K-feldspar, apatite and titanite. Hedenbergite is locally altered to babingtonite, a hydrated calcic–ferrous–ferric–silicate (*Cepedal* et al., 2003), in association with quartz, calcite and Fe-rich epidote (up to Ps_{48}). The second retrograde stage is characterized by the formation of chlorite and prehnite, in addition to quartz and calcite. Pyrite, chalcopyrite, arsenopyrite, and pyrrhotite (which is normally replaced by secondary pyrite and marcasite) are present in the retrograde proximal garnet-pyroxene skarn. Sulfides in the massive pyroxene skarn are mainly Fe and Cu–Fe-sulfides; pyrrhotite is only locally present. Bornite and chalcocite-digenite are more abundant in the wollastonite zone. Accessories are sphalerite, stannite, magnetite, molybdenite and tetrahedrite group minerals. Gold mineralization and accompanying TSB minerals are always associated with Fe–Cu sulfides, never with Fe-sulfides.

The magnesian Cu–Au skarn is characterized by an alternation of diopside ($Hd_{4–28}$)- and forsterite ($Fo_{73–91}$)-skarns, in which the proportion of pyroxene increases towards the igneous rock contact. Serpentine, tremolite, phlogopite, talc, quartz, calcite, K-feldspar, chlorite and apatite, together with ore minerals, formed during the retrograde skarn stage. Forsterite skarn is normally replaced by abundant hydrous Mg(±Fe)-silicates (serpentine, talc, iddingsite) in addition to tremolite,

phlogopite, magnetite and sulfides. There are two different sulfide assemblages: chalcopyrite ± bornite and pyrrhotite + chalcopyrite, the latter being located mainly in the outer zones of the magnesian skarn. Similarly to the calcic skarn, gold mineralization in magnesian skarn is also associated with chalcopyrite and bornite, and is never found associated with pyrrhotite. Alteration by Ag-rich residual fluids resulted in electrum with a very low Au-content, along with secondary Ag-minerals such as stromeyerite (AgCuS) and mckinstryite $(Ag,Cu)_2S$ (*Cepedal*, 2001).

At the El Valle deposit, temperatures obtained for prograde skarn formation, based on the composition and stability fields of major calc-silicates, in addition to the fluid inclusion study, were between 600 and 700 °C, for a confining pressure of around 1 kbar (*Cepedal* et al., 2000; *Cepedal*, 2001). The stability fields obtained taking into account the average composition of prograde skarn minerals, garnet (Grs_{60}) and pyroxene (Hd_{40}), and their alteration products, ferroactinolite (Tr_{43}) and epidote (Ps_{27}) (*Berman*, 1991), indicate maximum temperatures of the first retrograde stage of around 450 °C (*Cepedal*, 2001). Homogenization temperatures obtained from the fluid inclusion study for the retrograde alteration lie between 520 and 225 °C (*Cepedal* et al., 2000). Moreover, this study indicated an unmixing process, which generated two different fluids: a high-salinity aqueous fluid and a low-salinity volatile-rich fluid. The range of temperatures estimated for this unmixing process was between 425 and 350 °C. This fluid immiscibility could have played an important role in sulfide deposition. As regards the second retrograde stage, the temperatures obtained from chlorite geothermometry (chlorite has 59–67 mol.% chamosite) range from 280 to 335 °C (*Cepedal* et al., 2000), using the calibrations of *Cathelineau* (1988) and *Walshe* (1986). Although application of this geothermometer is regarded as controversial, these data are in accordance with the temperatures obtained from the fluid inclusion study and the stability field of prehnite at 1 kbar (*Berman*, 1991).

The Ortosa intrusion and the Au-reduced calcic skarn of the Ortosa deposit

The Ortosa intrusion, the northernmost igneous complex within the Río Narcea Gold Belt (Fig. 1), consists of a main stock and several dykes and sills outcropping in an elliptical area of about 1 km^2 (Fig. 2b). The igneous rocks vary in composition between monzogranite and quartz-monzodiorite. The latter is ilmenite-bearing and has a remarkably reduced character (*Martín-Izard* et al., 2000a). The host rocks consist of a siliclastic Upper Silurian formation with some interbedded carbonates, and the early Devonian Rañeces carbonate Group. Skarn metasomatism and associated gold mineralization overprinted these sedimentary and igneous rocks, forming endo- and exoskarns.

The earliest alteration stage generated potassium metasomatism that resulted in transformation of the siliciclastic rocks around the intrusion to biotite hornfels. In the endoskarn, the first metasomatic mineral to form is actinolite as a replacement of igneous ortho- and clinopyroxenes and biotite. Subsequently, quartz, pyroxene ($Hd_{30–45}$), and sulfides formed, followed by a second amphibole generation (ferroactinolite-ferrohornblende). The exoskarn is a commonly banded pyroxene-garnet skarn. Prograde minerals are pyroxene ($Hd_{10–30}$, up to 1.8% Jo) and garnet ($Gr_{71–85}$). The retrograde mineralogy consists of hedenbergite-rich pyroxene

(Hd_{50-87}, up to 3.5% Jo) and amphibole (ferroactinolite-ferrohornblende) that also replaces the retrograde pyroxene. Other minerals are quartz, K-feldspar, fluorapatite (abundant in association with amphibole), albite, epidote-clinozoisite, and calcite. A final stage of retrograde alteration produced pervasive silicification and carbonatization; amphibole is partially altered to chlorite.

Ore minerals in the Ortosa skarn are coeval with the retrograde mineral assemblages. The earliest formed sulfides, mainly associated with the hedenbergite-rich pyroxene and amphibole, are löllingite and pyrrhotite. These minerals occur within idiomorphic arsenopyrite as inclusions that often define the morphology of the previous crystals, indicating replacement (*Fuertes-Fuente* et al., 2000). Pyrrhotite continued to form during and after arsenopyrite crystallization. Two main types of ore are observed: one in which the arsenopyrite is the more abundant mineral, and the other one in which pyrrhotite is dominant. Where chalcopyrite is present, it corrodes and partially replaces the pyrrhotite. Sphalerite and stannite also occur in association with chalcopyrite. Pyrrhotite is locally associated with pyrite, but the latter more commonly occurs as an alteration product of pyrrhotite, along with marcasite.

The fluid inclusion study carried out by *Campa* et al. (2001) on ore samples from the Ortosa deposit showed the coexistence of two different fluids: a brine trapped in the multiphase fluid inclusions and a carbonic-rich vapor represented by aqueous-carbonic fluid inclusions. According to *Campa* et al. (2001), both fluids are likely to be the result of an unmixing process due to a gradual cooling from more than 540 °C down to 280 °C. The range of temperatures obtained using the composition of arsenopyrite (from 34.5 to 35.5 wt.% As) and the geothermometer of *Kretschmar* and *Scott* (1976), *Sharp* et al. (1985) is between 470° and 535 °C. For these calculations coexistence of arsenopyrite and löllingite was assumed (*Fuertes-Fuente* et al., 2000). The sulfur fugacity during the main period of deposition of the earliest ore minerals was constrained by the composition and stability fields of major calc-silicate and sulfide minerals (*Fuertes-Fuente* et al., 2000). The common occurrence of hedenbergite, pyrrhotite, arsenopyrite and löllingite and the absence of an andradite-quartz-pyrrhotite assemblage limit $\log fS_2$ to the range -9 to -6.5 log units. Oxygen fugacity is limited by the presence of pyrrhotite with hedenbergite and the absence of magnetite, resulting in a $\log fO_2$ lower than -22 log units (*Fuertes-Fuente* et al., 2000).

Au–Bi–Te assemblages

In order to establish the different Au–Bi–Te assemblages, we studied 38 ore samples from the El Valle calcic and magnesian skarns and the Ortosa calcic skarn. In the following section, we describe the petrology, mineralogy and phase relationships of the studied samples, which are grouped according to deposit type and localization within each deposit, in addition to the main co-existing sulfides.

Analytical methods

The mineralogical study was carried out using reflected-light polarizing microscopes, a CAMEBAX SX-50 electron microprobe and scanning electron microscopy in association with chemical microanalysis using energy dispersive X-ray (EDAX).

In all electron microprobe analyses, the standard deviation of results is less than 0.1%. Major and minor elements were determined at 20 kV accelerating potential, 20 nA beam current and acquisition time between 10 and 20 seconds for X-ray peak and background. The effective probe size was between 1 and 2 μm. The following X-ray lines were used: Au$L\alpha$ Ag$L\alpha$, Bi$M\alpha$, Hg$L\alpha$, Sb$L\alpha$, Pb$M\alpha$, Fe$K\alpha$, Cu$K\alpha$, Zn$K\alpha$, Cd$L\alpha$, Ni$K\alpha$, Co$K\alpha$, Te$L\alpha$, S$K\alpha$, Se$L\alpha$, As$L\alpha$. The standards employed were: FeS_2, $PdTe_2$, Ag, Cd, Sb_2S_3, PbS, Bi, Co, Ni, $CuFeS_2$, ZnS, $AuTe_2$, $PtTe_2$, Au, HgS, Te_2S, AsGa, Cu_2Se. All the analyses were performed at the University of Oviedo.

Description of samples from the El Valle calcic skarn

Pyrite-bearing mineralization

The single sample that is representative for the Au–Bi–Te association in this type of ore is from a proximal garnet-pyroxene skarn, in which garnet is partially

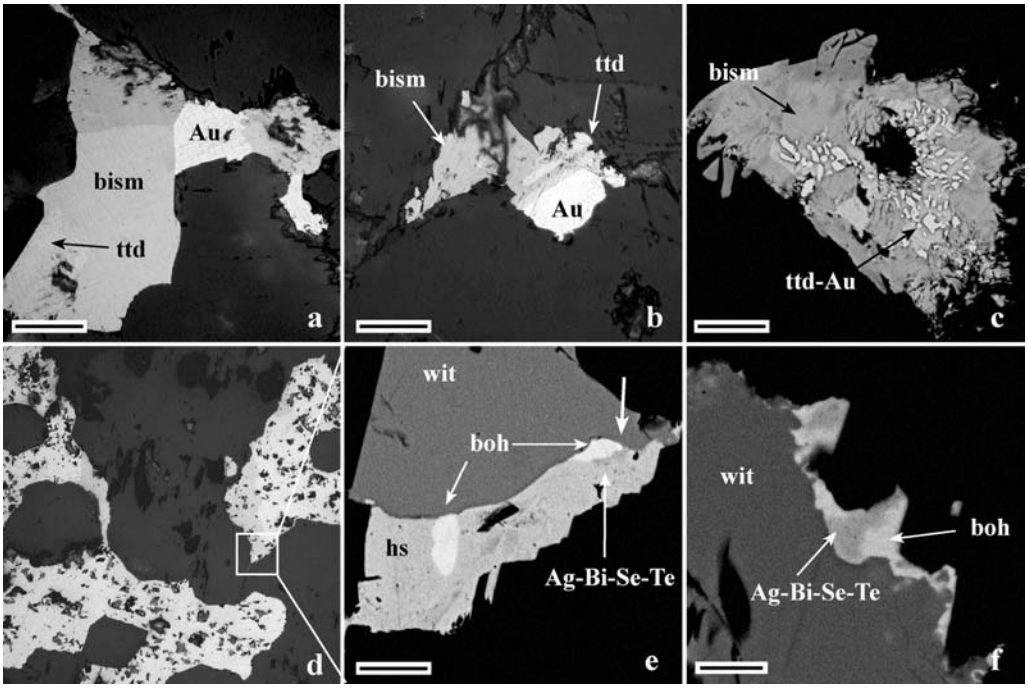

Fig. 3. Photomicrographs (**a**, **b**, and **d**) and back scattered electron images (**c**, **e**, and **f**) of telluride, selenide and sulfosalt assemblages from the El Valle calcic skarn. (**a**) and (**b**) Native gold associated with bismuthinite (bism) and tetradymite (ttd). Note the triple junction between the three minerals in **a**. Scale bars: 25 μm. (**c**) Symplectitic intergrowth between native gold and tetradymite hosted by bismuthinite. The grain is rimmed by aikinite (ai, dark gray), which is in turn partially intergrown with bismuthinite. Scale bar: 20 μm. (**d**) Chalcopyrite with marginal wittichenite (wit) and hessite (hs). (**e**) Detail of area marked in **d** showing bohdanowiczite (boh, white) lamellae within hessite. An unidentified Ag–Bi–Se–Te phase (medium gray) is present at the contact between hessite and bohdanowiczite. The arrow shows coloradoite (?). (**f**) Intergrowth between the Ag–Bi–Se–Te phase and bohdanowiczite. Scale bar for **e** and **f**: 15 μm

retrogressed to epidote, quartz and calcite, and pyroxene was partially altered to amphibole. As mentioned above, this skarn alteration is normally barren, with pyrite as the main sulfide. However, this sample has an anomalous high concentration of gold, together with a TSB assemblage mainly consisting of bismuthinite (Bi_2S_3) and tetradymite (Bi_2Te_2S) (Fig. 3a, b). Aikinite ($PbCuBiS_3$) is also found, but occurs in smaller amounts (Fig. 3c). These minerals occur isolated or in aggregates along with gold, infilling pores or cleavage planes of the skarn silicates, and occurring in quartz and calcite veins that crosscut and partially replace the skarn minerals. However, they are never observed with pyrite.

Grain boundaries between gold, bismuthinite and tetradymite are curved or slightly interpenetrated (Fig. 3a, b). Occasionally, gold forms disseminated dropslets in tetradymite (Fig. 3c). Aikinite, the presence of which was only detected by SEM, is sometimes associated with bismuthinite (Fig. 3c). Microprobe analyses of gold grains (Table 1) showed the highest fineness of El Valle skarn samples of between 825 and 975 FN [$FN = 1000^{*}Au/(Au + Ag)$], which indicates the presence of both electrum and native gold. Microprobe analyses of bismuthinite (Table 1) showed variable concentrations of Pb (from 0.6 to 4.0 wt.%) and Cu (up to 1.5 wt.%).

Table 1. *Selected analyses (number of analyses in brackets) of minerals in the pyrite-bearing assemblages from the El Valle calcic skarn*

Wt.%	Tetradymite		Bismuthinite		Aikinite			Electrum	
	(n = 8)		(n = 12)		(n = 3) (*)			(n = 6)	
Te	35.12	34.92	–	–	–	–		–	–
Ag	0.08	–	–	–	–	–		2.47	17.50
Au	–	0.17		–	–	–		96.29	82.53
S	4.74	4.89	18.90	18.70	15.90	16.09		–	–
Fe	0.22	0.76	–	0.23	–	–		–	0.29
Cu	–	–	1.45	0.84	10.83	8.27		0.15	–
Se	–	–	0.20	–	–	–		0.77	0.32
Sb	0.20	0.21	0.66	0.27	–	–		–	–
Hg	–	0.15	–	–	–	–		0.17	0.57
Pb	–	–	4.78	2.43	40.01	37.66		–	–
Bi	58.81	59.23	73.26	77.48	33.26	37.98		0.62	0.54
Total:	99.17	100.33	99.25	99.95	100.00	100.00		100.47	101.75
	to 6 atoms		to 5 atoms		to 6 atoms				
Bi	2.00	1.99	1.77	1.89	0.94	1.10			
Cu	0.00	0.00	0.12	0.07	1.00	0.78	FN	975	825
Pb			0.12	0.06	1.14	1.10			
Te	1.93	1.95							
Se	0.00	0.00	0.01						
S	1.07	1.05	2.98	2.98	2.92	3.02			

–: below minimum detection limits; (*): SEM-EDAX analyses; all the others by electron microprobe; FN: gold fineness

Chalcopyrite-rich mineralization

The four studied samples are from mineralized pyroxene skarn that consists of an early Fe-poor pyroxene (Hd_{12-37}, up to 0.6% Jo), partially replaced by a Fe-rich pyroxene (Hd_{75-96}, up to 5.3% Jo) and quartz. Pyroxene is first altered to ferroactinolite (Tr_{20-30}) and lastly to chlorite. Others minerals are quartz, calcite, K-feldspar and ore minerals, mainly chalcopyrite with smaller amounts of magnetite and molybdenite.

Gold occurs as Ag-rich electrum (573–618 FN). Other minerals found in association with electrum are wittichenite (Cu_3BiS_3), hessite (Ag_2Te), stützite (Ag_7Te_4), Bi-rich tetrahedrite [$(Cu,Fe)_{12}(Sb,As,Bi)_4S_{13}$], and bohdanowiczite ($AgBiSe_2$), among others that are described below. Wittichenite and hessite are the most common accessories and are commonly associated. Wittichenite occurs as relatively coarse (up to 500 μm) granular aggregates on grain margins of chalcopyrite (Fig. 3d, e), or in small blebs (≈30 μm) enclosed in chalcopyrite or gangue minerals. Microprobe data (Table 2) indicate the presence of Ag (to 2.83 wt.%) and Se (to 1 wt.%). Hessite also occurs on grain margins of chalcopyrite, in spatial association with wittichenite, or as isolated rounded grains enclosed in chalcopyrite or gangue. Microprobe analysis (Table 2) showed erratic contents of Cu and Fe that could be due to the neighboring chalcopyrite, and the presence of Se (to 1.7 wt.%), Sb (to 0.3 wt.%) and Hg (to 0.7 wt.%). Bohdanowiczite occurs as thin elongated lamellae within hessite (Fig. 3e). Only a single microprobe analysis is considered of sufficiently good quality to confirm this mineral (Table 2), due to the small size (<10 μm) of these grains. Even in this case, however, the analysis shows partial substitution of Se by Te (1.36 wt.% Te), which could be contamination from adjacent hessite.

We used back-scattered electron (BSE) imaging and EDX to investigate mineral relationships and assess the compositions of the smaller grains. Some of the hessite grains showed areas richer in Te (e.g. 41.85 wt.% Te, 58.15 wt.% Ag) that could correspond to stüzite instead of hessite. Moreover, BSE images showed a distinct, different phase at the contact between bohdanowiczite and hessite (Fig. 3e). The EDX analyses indicate an intermediate composition between these two minerals (Table 2), with significant substitution of Te by Se, ranging from 9 to 11.9 wt.%, and a very different ratio of Ag to Bi. This Te–Se phase was observed on several occasions (Fig. 3f). A Hg-rich telluride was detected by SEM-EDX analyses, but the extremely small size of this mineral (<1 μm, Fig. 3e) prevented its identification. The presence of coloradoite (HgTe) associated with hessite in other skarn samples from the El Valle deposit suggests that it may be this mineral.

Bornite-rich mineralization

The 5 studied samples are from a garnet (Adr_{37-43}), pyroxene (Hd_{28-56}) and wollastonite skarn that evolved into a pyroxene and wollastonite skarn. These samples show little retrograde alteration with ferroactinolite, babingtonite, prehnite, chlorite, in addition to quartz and calcite and ore minerals. These ore minerals are mainly Cu–(Fe)-sulfides (bornite and chalcocite ± digenite), which are interstitial between skarn minerals or infill veinlets along with quartz and calcite. Bornite is replaced by other Cu-sulfides, which are also intergrown with bornite, both in

Table 2. *Selected analyses (number of analyses in brackets) of minerals from chalcopyrite-rich assemblages in the El Valle calcic skarn*

Wt.%	Bi-rich Tetrahedrite		Wittichenite		Hessite		Bohdanowiczite			Ag–Bi–Se–Te	
	(n = 2)		(n = 12)		(n = 7)		(n = 1)	(n = 3) (*)		(n = 2) (*)	
Te	–	–	0.09	–	34.96	34.35	3.87	–	–	9.00	11.90
Ag	0.12	0.70	1.73	1.39	60.31	60.24	25.78	26.67	25.32	58.32	59.88
Au	–	–	–	–	0.06	0.07	–	–	–	–	–
S	24.14	24.26	18.88	19.37	0.15	0.08	1.36	–	–	–	–
Fe	2.02	2.43	0.25	0.40	1.25	1.58	0.57	–	–	0.72	–
Cu	37.18	36.91	36.24	36.66	1.32	0.47	0.83	1.96	–	–	–
Ni	–	–	–	–	–	–	–	–	–	–	–
Co	0.07	–	–	–	–	–	–	–	–	–	–
Zn	4.69	4.29	–	–	–	–	–	–	–	–	–
As	0.96	1.09	–	–	–	–	–	–	–	–	–
Se	0.24	0.21	0.66	0.56	1.71	0.76	24.79	31.04	31.78	22.89	21.32
Sb	23.61	25.62	–	–	0.18	0.30	–	–	–	–	–
Hg	–	–	–	0.22	0.40	0.38	0.29	–	–	–	–
Pb	–	–	–	–	–	–	–	–	–	–	–
Bi	5.01	3.63	42.01	41.55	–	–	41.35	40.33	42.90	7.61	6.91
Cd	0.86	0.33	–	–	–	–	–	–	–	–	–
Total	98.90	99.47	99.86	100.15	100.34	98.23	98.84	100.00	100.00	98.54	100.01
	to 29 atoms		to 7 atoms		to 3 atoms		to 4 atoms				
Cd	0.13	0.05									
Zn	1.23	1.12									
As	0.22	0.25									
Sb	3.33	3.59									
Bi	0.41	0.30	1.01	0.99			0.93	0.89	0.97	0.15	0.14
Ag	0.02	0.11	0.08	0.06	1.85	1.91	1.13	1.14	1.11	2.22	2.33
Cu	10.05	9.90	2.87	2.87	0.07	0.03	0.06	0.14	0.00	0.09	0.00
Fe	0.62	0.74	0.02	0.04	0.07	0.10	0.05	0.00	0.00	0.05	0.00
Te			0.00		0.91	0.92	0.14	0.00	0.00	0.29	0.39
Se	0.05	0.05	0.04	0.03	0.07	0.03	1.48	1.82	1.91	1.19	1.14
S	12.93	12.90	2.97	3.01	0.02	0.01	0.20	0.00	0.00	0.00	0.00

–: below detection limits; (*) SEM-EDAX analyses; all others by electron microprobe

random orientation and along cleavages (Fig. 4a). In these samples, both chalcopyrite and pyrite are scarce. Pyrite typically occurs as irregularly-shaped grains enclosed within bornite. This suggests that pyrite was partially replaced by bornite. Hematite, when it occurs, is found along the margins of the sulfides.

Accessory minerals are mainly Ag and Au-tellurides, electrum and members of the tetrahedrite group. They occur as rounded or irregular grains at the margin of Cu–(Fe)-sulfides and, less frequently, enclosed within gangue. Hessite and petzite (Ag_3AuTe_2) are the most abundant Au–Ag-tellurides. They occur as small grains (up to 20 μm), often in association with electrum, which is Au-rich (from 834 to 882 FN). Fine aggregates with electrum in the core surrounded by

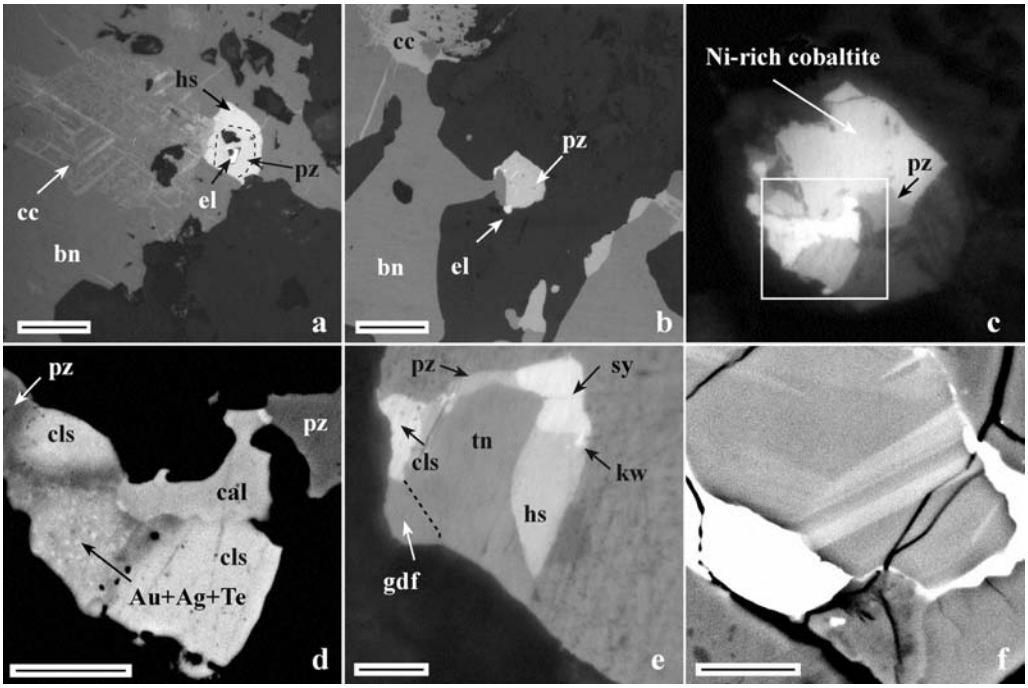

Fig. 4. Photomicrographs (**a**, **b**, **c**, and **e** under oil immersion) and back scattered electron images (**d** and **f**) of telluride, selenide and sulfosalt assemblages from the El Valle calcic skarn. (**a**) Electrum (el) rimmed by petzite (Pz) and outer hessite (hs) in bornite (bn); the latter is partially replaced along cleavages by Cu-sulfides (chalcocite–digenite, cc). Scale bar: 80 μm. (**b**) Petzite at the margin of bornite: electrum is present along cracks in petzite. Scale bar: 60 μm. (**c**) Ni-rich cobaltite grain corroded by Au–(Ag)-tellurides (cal: calaverite, pz: petzite) and clausthalite (cls) – shown in detail in **d**. Scale bar: 5 μm. (**e**) Aggregate of precious metal tellurides (hessite, sylvanite (sy), petzite), clausthalite, tennantite (tn), and goldfieldite (gdf) at the margin of bornite with replacement of chalcocite–digenite (not marked on the figure). Small grain of kawazulite (kw) enclosed in hessite. Scale bar: 8 μm. (**f**) Tennantite with compositional zonation: As-poor (bright) and As-rich tennantite (gray). Scale bar: 5 μm

petzite and marginal hessite (Fig. 4a) may represent the decomposition products of sylvanite, $(Au,Ag)_2Te_4$. Elsewhere, electrum fills microfractures in petzite grains (Fig. 4b). Microprobe analyses carried out on hessite grains show a variation between the proportion of Te and Ag, again indicating the possible presence of stützite (Table 3).

Sylvanite and calaverite ($AuTe_2$) are the other Au–Ag-tellurides present (Fig. 4c–e). Electron probe microanalyses show that sylvanite is Ag-rich (Table 3), with little variation in Ag content (from 11.2 to 13.8 wt.%). This Ag-rich sylvanite is to be expected where it forms in equilibrium with petzite (e.g., *Shackleton* et al., 2003), which is consistent with our petrographic observations. Nevertheless, some analyses show a significant Cu content (>3 wt.%; Table 3), which is linked to a decrease in the Au and, especially, Te content. Calaverite is much less common, and was only observed in a single sample. It occurs in association with petzite and clausthalite, partially corroding a crystal of Ni-rich cobaltite (Fig. 4c, d). The small

Table 3. *Representative analyses (number of analyses in brackets) of minerals in the bornite-rich assemblage from the El Valle calcic skarn*

Wt.%	Hessite	Stützite	Sylvanite	Petzite	Calaverite	Clausthalite		Ni-rich Cobaltite		Goldfieldite		Tennantite
	(n = 8)	(n = 2)	(n = 5)	(n = 9)	(n = 2)(*)	(n = 3)		(n = 4)		(n = 4)		(n = 9)
Te	37.19	39.97	61.63	30.91	57.74	0.73		–	Te	11.70	–	0.97
Ag	61.14	56.65	11.18	42.19		0.15		–	Ag	0.03	–	0.45
Au	–	–	24.80	25.07	42.26	0.84		–	Au	–	–	0.28
S	–	–	0.15	–		2.53		17.73	S	25.74	24.49	26.34
Fe	–	0.31	0.10	0.30		0.54		3.03	Fe	0.40	0.31	0.22
Cu	0.54	2.11	0.84	0.67		–		1.14	Cu	46.54	37.97	41.58
Ni	–	–	–	–		0.11		10.17	Ni	–	–	–
Co	–	–	–	–		–		22.91	Co	–	–	–
Zn	–	–	–	–		0.12		–	Zn	1.26	6.88	6.74
As	–	–	–	0.16		–		43.67	As	9.52	9.39	14.07
Se	–	0.11	–	0.72		22.22		–	Se	0.39	0.13	–
Sb	0.16	0.31	0.37	0.18		–		–	Sb	3.30	10.64	6.61
Hg	0.18	–	0.39	–		–		0.26	Hg	–	–	–
Pb	–	0.20	–	–		72.22		–	Pb	–	–	–
Bi	–	–	–	–		–		–	Bi	–	8.64	0.96
Cd	0.69	–	0.20	–		–		–	Cd	–	1.44	1.57
Total	99.90	99.66	99.66	100.20	100.00	99.46		98.91	Total	98.88	99.89	99.79
	to 3 atoms	to 11 atoms	to 6 atoms		to 3 atoms	to 2 atoms		to 3 atoms		to 29 atoms		
Pb						0.98			Bi		0.69	0.07
Au	0.00	0.00	1.03	0.98	1.04		Ni	0.29	Cd		0.21	0.22
Ag	1.95	6.54	0.85	3.00	0.00		Co	0.66	Ag		0.00	0.06
Cu	0.03	0.41	0.11	0.08	0.00		Cu	0.03	Cu	11.71	9.96	10.23
Te	1.00	3.90	3.95	1.86	2.03	0.02	Fe	0.09	Fe	0.12	0.09	0.06
Se	0.00	0.02	0.04	0.01	0.00	0.79	As	0.99	Zn	0.31	1.75	1.61
S	0.01	0.02	0.00	0.07	0.00	0.22	S	0.94	As	2.03	2.09	2.94
									Sb	0.43	1.46	0.85
									Te	1.48	0.00	0.12
									Se	0.08	0.03	0.00
									S	12.84	12.72	12.84

–: below minimum detection limits; (*): SEM-EDAX analyses; all others by electron microprobe

size of the calaverite grains (<7 μm) did not allow us to obtain good microprobe analysis; EDAX data nonetheless indicate that Ag is absent in calaverite (Table 3).

Other minerals present are clausthalite (PbSe) and kawazulite (Bi_2Te_2Se). Clausthalite is, in some of the samples studied, a relatively abundant mineral. It occurs in association with Au–(Ag)-tellurides (hessite, petzite, sylvanite and calaverite, Fig. 4d and e). Electron microprobe analyses indicate a partial substitution of Se by S and Te (Table 3). Kawazulite, in contrast, is very scarce. It occurs as small grains (<10 μm), always enclosed by hessite (Fig. 4e). This fact suggests that this mineral was formed by exsolution from hessite. The small size of the grains of this mineral did not allow us to obtain good microprobe analyses, but its occurrence was also confirmed by SEM-EDX. Electron probe microanalyses also indicated the presence of coloradoite associated with hessite.

Minerals of the tetrahedrite group, $Cu_{12}(As,Sb,Bi)_4S_{13}$, occur as relatively coarse grains, rimmed by Ag–Au-tellurides (Fig. 4e, f). Tennantite is the most abundant, with As content ranging from 9 to 14 wt.% (Table 3). BSE images (Fig. 4f) show that these grains have a compositional zonation due to variation in As content. Microprobe analyses indicate significant concentrations of Bi from 1 to 8.6 wt.%, showing an inverse relation between Bi and As contents. Another notable impurity is Cd (typically around 1.5 wt.%) (Table 3). Also, some microprobe analyses indicate the presence of minor goldfieldite [$Cu_{12}(Te,Sb,As)_4S_{13}$] (Table 3, Fig. 4e).

Other accessory minerals include a phase from the cobaltite (CoAsS) – gersdorfite (NiAsS) solid solution, as mentioned above. The chemical composition is closer to the Co-rich end member, i.e. Ni-rich cobaltite (Table 3). It is very scarce and small in size (20–40 μm), and appears enclosed within Cu-sulfides and bornite and is partially corroded by the tellurides, selenides and tetrahedrite group minerals (Fig. 4c).

In contrast to the other associations from the calcic skarn, wittichenite is rather rare in bornite-rich ore. When present, it occurs as small grains intergrown with the Cu–(Fe)-sulfides that replace bornite, and never in association with the other trace minerals described above.

Description of samples from the El Valle magnesian skarn

As mentioned above, gold assemblages in the magnesian skarn are restricted to the occurrence of Cu–Fe-sulfides and the lack of pyrrhotite. Consequently, several samples of chalcopyrite- and bornite-rich ores were studied. These samples are hosted by forsterite (Fo_{85-92}) and diopside (Hd_{4-28}) magnesian skarn intensely altered to tremolite, hydrous Mg- and Fe-silicates (serpentine, talc, iddingsite), phlogopite and dolomite. In these samples, the bornite/chalcopyrite ratio is variable. There are samples where chalcopyrite is almost the only Cu–Fe-sulfide. By contrast, other samples show a bornite/chalcopyrite ratio close to 1. On these occasions, chalcopyrite forms spindle-shaped grains or replacements along grain boundaries and fractures in the bornite crystals. In those samples with similar proportions of chalcopyrite and bornite, both minerals show complex relationships, and frequently occur as fine-scale symplectitic intergrowths (Fig. 5a). Magnetite is present as tiny inclusions in olivine crystals and as subhedral to anhedral grains

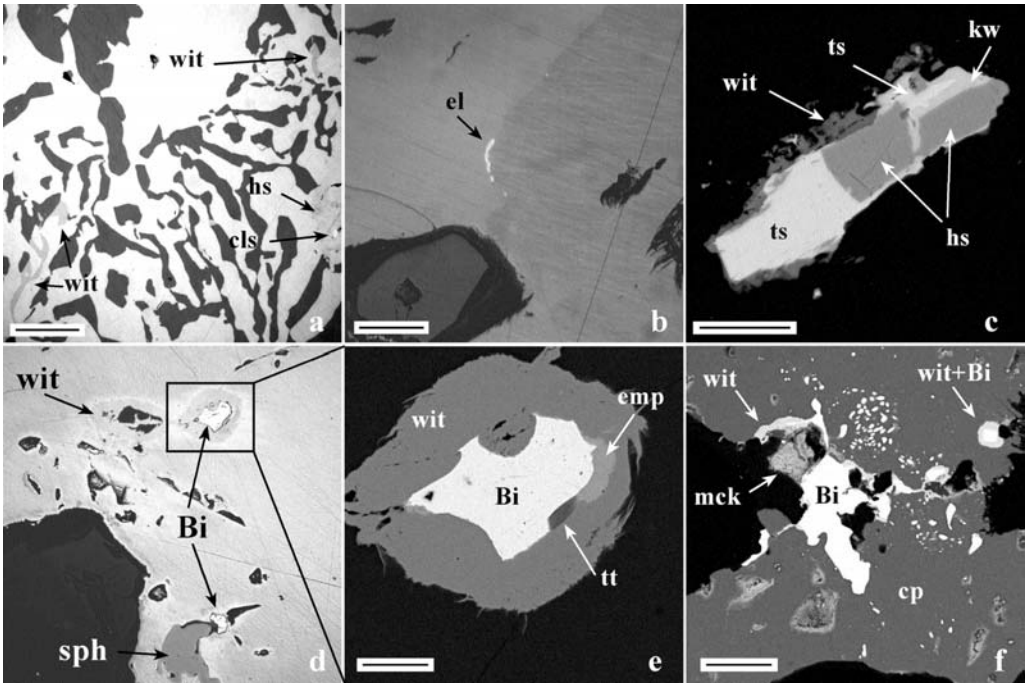

Fig. 5. Photomicrographs (**a**–**d**) and back scattered electron images (**e** and **f**) of telluride, selenide and sulfosalt assemblages from the El Valle magnesian skarn. (**a**) Symplectitic intergrowth between chalcopyrite (dark), bornite ± wittichenite (wit) and hessite (hs). Scale bar: 160 µm. (**b**) Ribbon-like electrum (el) located at the contact between two bornite grains. Scale bar: 10 µm. (**c**) Patch of hessite, tsumoite (ts) and kawazulite (kw) rimmed by wittichenite. Scale bar: 10 µm. (**d**) Radiating aggregates of wittichenite surrounding native bismuth and voids in chalcopyrite. Sphalerite (sph) is also present in chalcopyrite. (**e**) Detail of area marked in **d** showing emplectite (emp) and Bi-rich tetrahedrite (tt) at the contact between native bismuth and wittichenite. Scale bar: 12 µm. (**f**) Chalcopyrite (cp) with exsolved blebs of native bismuth (white); coarser grains of native bismuth surrounded by wittichenite. Fine-grained areas with mckinstryite (mck) occur at the margin of chalcopyrite. Scale bar: 25 µm

enclosed and partially corroded by Cu–Fe-sulfides. Also, these sulfides are rimmed by magnetite as a product of subsequent skarn alteration. The accessory minerals found are different, depending on whether bornite or chalcopyrite is the main sulfide.

Bornite-rich ore samples

In the 4 studied samples, the accessory minerals found are wittichenite, hessite, electrum, native bismuth, coloradoite, tsumoite (BiTe), kawazulite, clausthalite and Ni–Co–As–Sb–S minerals. Wittichenite and hessite are the most abundant. They appear as rounded or ribbon-like grains at the boundary of the sulfide grains or around voids within these grains. They are also located at the contact between two bornite grains or at the contact of the replacement rims of bornite by chalcopyrite. This distribution suggests that these phases exsolved directly from bornite during

cooling. Moreover, wittichenite and hessite appear in the symplectitic intergrowths between bornite and chalcopyrite (Fig. 5a). Gold mainly occurs as low-Au electrum (417–530 FN). Electrum commonly appears as bleb or ribbon-like inclusions located at the contact between bornite grains (Fig. 5b). It is commonly associated with wittichenite and hessite. Gold grains with higher Au content (up to 900 FN) were also found. The particularity of this gold is that it appears as isolated grains, filling interstices between skarn minerals, and has a significant Cu content (up to 6.5 wt.%). This Au–Cu–Ag alloy was probably deposited at high temperature along with the bornite, whereas the gold without Cu seems to be an exsolution product from cooling bornite. Native bismuth is present only in some samples and with a similar distribution to that of electrum. Tellurides and selenides (coloradoite, clausthalite, tsumoite and kawazulite) are less abundant and are commonly associated with hessite (Fig. 5c).

Chalcopyrite-rich ore

In the 3 studied samples, the accessory minerals found are: Bi-sulfosalts, electrum, native bismuth, bismuthinite, hessite and Bi-bearing tetrahedrite; as well as sulfides such as sphalerite and cobaltite. Sphalerite is infrequent but occurs in coarse and irregular grains enclosed in chalcopyrite (Fig. 5d). Wittichenite is the most abundant Bi-sulfosalt and sometimes occurs around other minerals such as native bismuth, electrum or hessite (Fig. 5d, e). Emplectite ($CuBiS_2$), when present, is associated with wittichenite, especially where wittichenite surrounds native bismuth (Fig. 5f). Emplectite occurs at the contact between these two minerals and seems to be a reaction product between native bismuth and wittichenite. In other cases, emplectite is intergrown with a Ag-rich phase (Table 4) that may correspond to an unnamed Ag-rich homologue in the cuprobismutite series, ideally $Cu_8(Ag_2Bi_{14})_{16}S_{26}$, characterized by a $Cu/(Ag + Bi)$ atom ratio of 8:16, similar to that described by *Cook* and *Ciobanu* (2003). However, in the specimen from El Valle, a greater amount of Bi is substituted by Ag and the Pb content is lower than that described by these authors.

Native bismuth is especially abundant in one of the studied samples. It occurs as swarms of minute blebs, as well as larger areas within chalcopyrite (Fig. 5f). Wittichenite commonly surrounds native bismuth, and is also associated with electrum, native silver and mackinstriyite, which occurs as dusty aggregates (Fig. 5f). Native bismuth does not coexist with bismuthinite in the sample where the latter was found; bismuthinite is only associated with electrum and hessite.

Electron microprobe data for Au–Ag–Bi–Te–S minerals from the El Valle magnesian skarn are summarized in Table 4. The chemical composition of wittichenite is similar to that in associations from the calcic skarn (Table 1). Both have comparable Ag contents, although wittichenite from magnesian skarn seems to contain less Se. The analyses of tsumoite show small substitutions of Te by Se and Bi by Ag. Other notable impurities are Fe and Cu, both of which are also present in the analyses of hessite and coloradoite. Compositional data for coloradoite show variable Ag contents, although it may be the influence of hessite, due to the fact that both minerals are always in association. Kawazulite was only analyzed by SEM-EDX, due to its small size ($<10\,\mu m$).

Table 4. *Selected analyses (number of analyses in brackets) of minerals in assemblages from the El Valle magnesian skarn*

Wt.%	Wittichenite		Emplectite		Ag-rich Bi-sulfosalt		Tsumoite		Coloradoite	Kawazulite
	(n = 7)		(n = 6)		(n = 6)		(n = 4)		(n = 3)	(n = 1) (*)
Te	0.13	–	–	–	0.17	0.07	34.12	34.38	39.28	36.85
Ag	0.43	1.43	0.32	2.29	6.00	6.71	0.16	0.06	2.90	–
Au	0.71	–	0.31	–	0.19	–	–	–	–	–
S	19.50	18.96	18.61	18.76	18.46	18.32	–	–	–	–
Fe	1.26	1.01	0.44	0.58	0.35	0.163	0.42	0.48	0.73	–
Cu	36.70	35.79	16.72	16.02	11.05	11.05	0.45	0.43	1.62	–
Ni	–	–	0.04	0.00	–	–	–	0.06	–	–
Co	–	–	–	0.10	–	–	–	–	–	–
Se	–	0.07	0.05	–	0.19	–	0.34	0.24	0.31	7.78
Sb	–	–	–	–	–	–	0.14	0.18	0.31	–
Hg	–	–	0.16	0.13	–	0.14	–	–	54.71	–
Pb	–	–	–	–	–	–	0.39	0.32	0.10	–
Bi	41.47	41.57	63.28	60.66	64.10	63.33	62.05	63.90	–	55.37
Total	100.19	98.83	99.94	98.54	100.51	99.78	98.07	100.05	99.96	100.00
	to 7 atoms		to 4 atoms		to 50 atoms		to 2 atoms		to 2 atoms	to 5 atoms
Hg									0.84	
Bi	0.98	1.00	1.05	1.00	13.71	16.60	1.01	1.03		2.03
Ag	0.02	0.07	0.01	0.07	2.48	2.79	0.00	0.00	0.09	
Cu + Fe	2.98	2.93	0.94	0.91	8.06	7.94	0.05	0.05	0.08	
Te	0.01				0.06	0.00	0.91	0.91	0.98	2.21
Se		0.00	0.00		0.11		0.02	0.01	0.01	0.76
S	3.02	2.99	2.01	2.02	25.75	25.65				

–: below minimum detection limits; (*): SEM-EDAX analyses; all the others by electron microprobe

Description of samples from the Ortosa skarn

We studied samples representative of the two main sulfide associations, the arsenopyrite-rich (5) and the pyrrhotite-rich (4) types, and samples where pyrite is associated with pyrrhotite (2). In these samples, gold occurs as electrum (from 533 to 885 FN), native gold and maldonite (Au_2Bi), and is mainly accompanied by hedleyite (Bi_7Te_3), native bismuth, and joséite-B (Bi_4Te_2S).

Arsenopyrite-rich ore

Minerals of the Au–Bi–Te–(Se) association occur at grain boundaries of arsenopyrite or inside arsenopyrite at the boundary of the löllingite or pyrrhotite inclusions (Fig. 6a–c). This association consists of native bismuth, which is the most abundant, gold as native gold or electrum, hedleyite, joséite-B, galena, maldonite and joséite-A (Bi_4TeS_2). Gold and native bismuth are commonly present as small (<40 μm), irregular grains located at the boundary of the löllingite inclusions in arsenopyrite. Gold and native bismuth, however, usually occur in association with

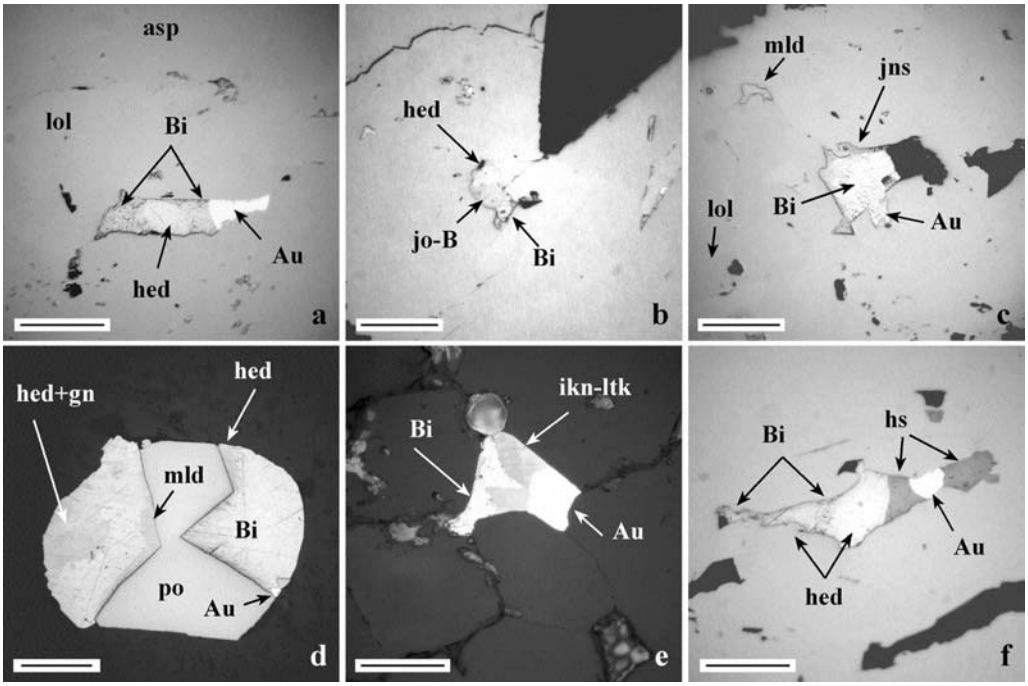

Fig. 6. Reflected light photomicrographs of Au–Bi–Te–S assemblages from the Ortosa deposit. (**a**) Elongated patch consisting of native bismuth, gold and hedleyite (hed) in löllingite (lol) located close to the contact with arsenopyrite (asp). Scale bar: 60 μm. (**b**) Composite inclusions with hedleyite, joséite-B (jo-B) and native bismuth in arsenopyrite. Scale bar: 60 μm. (**c**) Skeletal inclusions of maldonite (mld) and coarser patches of native bismuth in arsenopyrite. Tiny inclusions of native gold and also jonassonite (jns, light gray) are present in the native bismuth. Note also the löllingite relicts in arsenopyrite. Scale bar: 60 μm. (**d**) Polymetallic droplet consisting mainly of pyrrhotite (po), native bismuth and hedleyite. Native gold and maldonite are present as inclusions at the boundaries between the Bi-minerals and pyrrhotite. Hedleyite has <5μm inclusions of galena (gn). Scale bar: 70 μm. (**e**) Native bismuth, gold and ikunolite (ikn)-laitakarite (ltk) forming a patch interstitial to apatite. Scale bar: 30 μm. (**f**) Patch of native bismuth, gold, hedleyite and hessite (hs) enclosed in arsenopyrite. Scale bar: 60 μm

other minerals, forming aggregates of two or more different phases. The more frequent associations found are: (i) native bismuth and gold; (ii) native bismuth and hedleyite; (iii) native bismuth, hedleyite and gold (Fig. 6a); (iv) native bismuth, hedleyite and joséite-B (Fig. 6b); and (v) native bismuth and maldonite. Patches containing these minerals also occur interstitially between arsenopyrite crystals (Fig. 6c). Curvilinear boundaries between phases are observed in many of the aggregates. The third Bi-telluride (joséite-A, Table 5), is far less abundant than joséite-B.

A mineral with composition resembling the recently IMA-approved jonassonite, $Au(Bi,Pb)_5S_4$ (*Paar* et al., 2006) was observed in one sample. This mineral is light gray and tabular in shape, and occurs as a rim at the mutual contact between native bismuth and arsenopyrite (Fig. 6c). The chemical composition obtained by EDX is: 9.73 wt.% S, 67.23 wt.% Bi, 6.45 wt.% Pb and 16.59 wt.% Au. This is quite similar to that reported for an unnamed phase from Nagybörzsöny, Hungary (*Dobosi* and

Table 5. *Selected electron microprobe analyses (number of analyses in brackets) of minerals in the assemblages from the Ortosa deposit*

Wt.%	Maldonite		Hedleyite		Joséite-B	Joséite-A	Laitakarite	Ikunolite
	(n = 2)		(n = 15)		(n = 6)	(n = 1)	(n = 3)	(n = 3)
Te		19.09	21.90	23.09	21.51	13.82	0.32	–
Ag	0.16	–	–	–	–	–	–	0.18
Au	64.74	–	0.46	–	–	–	0.25	0.28
S	0.05	–	–	–	2.79	5.88	1.97	10.48
Fe	1.10	–	–	0.14	–	1.25	–	–
Cu	–	–	–	–	–	0.12	–	0.14
Zn	–	–	0.14	–	–	–	–	–
As	–	–	0.07	0.09	–	0.11	0.16	0.09
Se	0.43	–	0.22	0.11	0.69	0.33	18.06	0.16
Sb	–	1.03	0.13	0.23	0.41	0.11	–	–
Hg	–	–	0.18	0.26	–	–	–	–
Pb	0.26	–	–	0.36	–	1.20	–	–
Bi	32.83	79.68	76.42	76.13	73.54	76.34	79.45	88.85
Total	99.57	100.8	99.52	100.41	98.94	99.16	100.21	100.18
	to 3 atoms	to 10 atoms			to 7 atoms			
Au	2.03							
Bi	0.97	7.07	6.76	6.64	3.97	3.96	3.96	3.95
Sb		0.16	0.02	0.04	0.04	0.01		
Te		2.77	3.17	3.30	1.90	1.14	0.03	
Se			0.05	0.03	0.03	0.04	2.38	0.02
S					1.01	1.94	0.64	3.04

–: below detection limits

Nagy, 1989), although the Ortosa specimen has a higher Au content than the Hungarian one. Jonassonite is a rare Au–Bi–(Pb)–S mineral known only from a few occurrences (see *Jambor* and *Puziewicz*, 1990 and *Ciobanu* et al., 2006, this volume). Association of this mineral with Bi-tellurides, native bismuth, -gold, and maldonite, as in Ortosa, has been described from some of the previously-reported occurrences.

Pyrrhotite-rich ore

Typical assemblages include gold, native bismuth, hedleyite and joséite-B. Other minerals are maldonite, galena (PbS), ikunolite [$Bi_4(S,Se)_3$] and laitakarite [$Bi_4(Se,S)_3$]. These tellurides/selenides and Au minerals are found interstitially within gangue minerals. More commonly, however, they form polymetallic droplets with pyrrhotite or fill fractures crosscutting pyrrhotite grains (Fig. 6d). As in the arsenopyrite-rich samples, the most abundant trace mineral in the pyrrhotite ore is native bismuth, which occurs isolated, or in association with two or more other minerals. Selenium-bearing minerals, i.e. laitakarite and ikunolite (Table 5) in association with native bismuth and gold were observed in one patch (Fig. 6e).

This is interstitial to retrograde fluorapatite. Maldonite occurs with native bismuth and hedleyite at the border of pyrrhotite (Fig. 6d), and the contact between maldonite and native bismuth shows straight boundaries. Hedleyite contains sub-5 μm inclusions of galena.

Pyrite-bearing ore

In those samples where pyrrhotite appears partially replaced by pyrite and marcasite, the Au–Bi–Te assemblages show the same distribution as described above. In these samples, galena has been found forming coarse grains that fill cavities in arsenopyrite crystals, commonly associated with chalcopyrite. Hessite was identified, associated with Ag-rich electrum, hedleyite and native bismuth (Fig. 6f). In samples where pyrite is a primary mineral, gold grains were only observed as inclusions in pyrite crystals. Bismuthinite was also found associated with gold and native bismuth.

Selected microprobe analyses of the Au–Te–Bi minerals from the Ortosa skarn are compiled in Table 5. Analyses of hedleyite show significant compositional variation in both Te (from 18.0 to 23.1 wt.%) and Bi (from 75.3 to 78.3 wt.%); typical impurities are Sb and Se. Formulae calculations were done on the basis of 10 atoms (Bi_7Te_3), but as a result of an excess or deficiency of Te gives an apparent non-stoichometric formula. This fact suggests that $Bi_{2+x}Te_{1-x}$ is a more appropriate formula is, where x varies between 0.12 and 0.47. Analyses of native bismuth indicate that Sb is the most common impurity (up to 1.3 wt.%). Analyses carried out on Se-bearing minerals show a fairly continuous variation between ikunolite with extremely low Se/S and laitakarite. Also, the more Se-rich analyses show significant contents of Te (Table 5). In the bismuthinite analyses there is also a minor substitution of S by Se.

Discussion

Ore formation

At the El Valle deposit, the interstitial character of the Cu–Fe-sulfides with tremolite and phlogopite in the magnesian skarn and with actinolite-ferroactinolite in calcic skarn suggests the main stage of bornite and chalcopyrite crystallization is coeval with the first stage of retrograde skarn formation. In accordance with this, we estimate a formation temperature for Fe–Cu–S-sulfides of around 450 °C, but certainly not higher than 500 °C. The common presence of magnetite indicates geochemical conditions of sulfide formation within the magnetite stability field. The two different associations (chalcopyrite- and bornite-rich), may indicate small variations in terms of fS_2 and fO_2 as was suggested by *Cook* and *Ciobanu* (2001) for the Ocna de Fier-Dognecea Fe–Cu skarn, Romania.

The bornite-rich ore in calcic skarn relates to a slightly altered garnet (Adr_{37-43}), pyroxene (Hd_{28-56}) and wollastonite skarn, which has the characteristics of a porphyry-related calcic skarn (*Johnson* and *Norton*, 1985). These authors show that, in these types of skarn, magnetite is rare in association with wollastonite, whereas bornite and chalcocite are the only sulfides with which wollastonite can reach

equilibrium in the presence of quartz-saturated fluid. At low CO_2 concentrations ($XCO_2 < 0.05$), a requirement for formation of these skarns (*Johnson* and *Norton*, 1985), the minimum temperature necessary to form wollastonite at 1 kbar is around 470 °C (*Berman*, 1991). Bornite and chalcocite continued to form during the retrograde stage along with quartz and calcite, and hydrous calc-silicates, amphibole, prehnite and babingtonite. The latter mineral is stable over a wide range of fO_2 and is related to low-XCO_2 fluids (*Burt*, 1971; *Shvedenkov* and *Mazurov*, 1977), consistent with the data mentioned above. The lack of magnetite in this mineral association suggests that the crystallization of silicate minerals consumed most of the iron, increasing the Cu/Fe ratio and allowing the formation of Cu–(Fe)-sulfides (bornite, chalcocite ± digenite) (*Cepedal* et al., 2001). According to these authors, babingtonite would have acted as a fO_2 buffer, favoring sulfide precipitation. The presence of hematite in some samples indicates that fO_2 values reach the hematite-magnetite buffer.

Iron–Cu-sulfides and löllingite as carriers for TSB and/or precious metals

The close association of Fe–Cu-sulfides with gold suggests that it was initially deposited in solid solution in these sulfides. Experiments in the Cu–Fe–S–Au system show that Cu–Fe-sulfides can incorporate a large amount of gold in solid solution (*Simon* et al., 2000). At any temperature, bornite hosts about an order of magnitude more gold than chalcopyrite. The difference in the Au-hosting capacity of bornite and chalcopyrite is directly related to their Cu content, which is about 64 and 34%, respectively (*Kesler* et al., 2002). At 700 °C, the highest temperature for which data are available, bornite can host 700 ppm gold; the maximum gold content drops rapidly with decreasing temperature but the amount is still almost 10 ppm at 400 °C. The temperatures of Cu–Fe-sulfide formation obtained for the El Valle deposit, less than 500 °C, indicate that a part of the gold could have initially been present in solid solution within bornite, and was exsolved as the deposits cooled. This is supported by the occurrence of small gold grains at interfaces between bornite grains, or around voids within bornite grains, etc., and the occurrence of some grains of Au–Cu–Ag alloy, as noted above.

Similar textural relationships between chalcopyrite, bornite and wittichenite are observed, suggesting that the latter mineral may have formed due to the cooling of an initial Bi-bearing solid solution. The presence of Ag-minerals (e.g. hessite and the Ag-rich Bi-sulfosalt), in addition to the presence of Ag in wittichenite (Tables 2 and 4), indicates that the initial solid solution also carried Ag. Such intergrowths have been described on several occasions (e.g. *McQueen* and *Larson*, 1985; *Oen* and *Kieft*, 1976). According to the latter authors, these intergrowths were presumably formed by unmixing at high temperature (400–500 °C) of Ag–Bi-bearing $bornite_{ss}$.

The other minerals, tellurides and selenides, may have originated either as early segregations from $bornite_{ss}$, or as melt droplets and crystallized in equilibrium with the host (*Oen* and *Kieft*, 1984). The extensive variety of mineral phases in the bornite-rich ore may be a consequence of the capacity of bornite to accommodate large amounts of trace elements at high temperatures, and prolonged cooling has led to the formation of exsolved minerals.

In the Ortosa deposit, the distribution of native gold as inclusions in arsenopyrite surrounding relictic löllingite indicates that gold was released during the transformation of löllingite to arsenopyrite, equivalent to that diagnosed during retrograde metamorphism by *Tomkins* and *Mavrogenes* (2001). The same distribution of native bismuth grains at the interfaces between löllingite and arsenopyrite may indicate a similar origin for this native bismuth. As far as we are aware, however, there are no published data on the occurrence of native bismuth within löllingite.

Native bismuth and Bi-tellurides as Au-scavengers

Douglas et al. (2000) proved experimentally that liquid bismuth, if fractionated from a solution above its melting point, would incorporate Au even when the fluid is Au-undersaturated. Similarly, formation of Bi-tellurides from melts that are precipitated from fluids was discussed for different types of deposits with emphasis on the potential to attract Au enrichment (*Ciobanu* et al., 2005). These authors sustain that in such cases typical textures will include droplet-shaped inclusions and also mutual curvilinear boundaries between crystallized minerals within the inclusions. Furthermore, the curvilinear boundaries are indicative of associations formed at eutectic points in a melt system. If the assemblage is formed from a melt, the end products of crystallization will always represent eutectic associations in the considered system (and/or subsystems), i.e., the Au–Bi–Te–S system for the discussion here, even if the initial composition of the melt is different from that at the eutectic. Many Au skarns worldwide carry a Bi–(Te)-mineral trace signature that is interpreted in connection with the role played by the liquid Bi as Au scavenger during ore formation (e.g. *Meinert*, 2000).

The gold-tetradymite-bismuthinite(±aikinite) assemblages found in proximal calcic skarn in El Valle, show interstitial position with respect to the skarn silicates. They also display curved mutual boundaries and intergrowth textures (Fig. 3a–c) suggesting, as mentioned above, that these aggregates formed from initial Au–Bi–(Pb)–Te–(S) melts. In the Ortosa skarn native gold and -bismuth also form aggregates of two or more different phases with other trace minerals, commonly showing the same curvilinear mutual boundaries that may be indicative of melt precipitation as in El Valle. If true, Au and Bi-minerals were probably extracted from fluids as Au–Bi–Te–(S) melts at temperatures above the melting point of bismuth, and formed equilibrium assemblages (as crystallization reached eutectic points in the Au–Bi–Te–S system and/or individual sections of this system) with the bulk composition of the initial droplets. Such interpretation was previously given for Bi-mineral associations in deposits of magmatic-hydrothermal affiliation (e.g. Larga, Romania; *Cook* and *Ciobanu*, 2004).

Telluride/selenide assemblages as petrogenetic indicators

Despite the fact that tellurides, selenides and associated sulfosalts occur as small or very small grains, the presence of these minerals and their mutual relationships can be valuable indicators of ore formation conditions because they are highly sensitive to changes in environmental conditions (*Ciobanu* and *Cook*, 2002). Therefore, the different Bi-telluride associations reported from El Valle and Ortosa skarns reflect

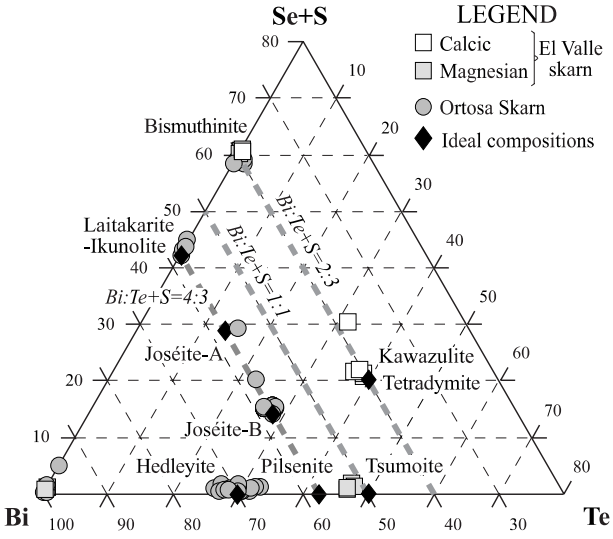

Fig. 7. Ternary Bi–Te–Se + S plot of the TSB minerals from the El Valle and Ortosa deposits

the different crystallization environments that existed in the two skarns during the formation of these minerals.

In terms of oxygen fugacity, in Ortosa, the speciation of Bi-tellurides with $Bi/Te(+Se+S) \geq 1$ (Fig. 7, hedleyite, joséite-B, -A, laitakarite-ikunolite) is consistent with a pyrrhotite-buffered environment. There is, however, no significant variation in the TSB assemblage found in different types of ore from Ortosa, suggesting similar fO_2 conditions across the entire deposit. In the El Valle skarns (both magnesian and calcic), the Bi-tellurides have $Bi/Te(+Se+S) \leq 1$ (Fig. 7), suggesting the more oxidized conditions of the magnetite stability field and proximity to the hematite-magnetite buffer (*Ciobanu* and *Cook*, 2002). This fact may explain the lack of Au–Bi assemblages co-existing with pyrrhotite. Contrary to the Ortosa skarns, a certain variation does, however, exist in the speciation of Bi-tellurides between calcic and magnesian skarn assemblages at the El Valle deposit. The Bi-tellurides (tetradymite and kawazulite) found in the calcic skarn have $Bi/Te(+Se+S) < 1$. In the magnesian skarn, the presence of tsumoite with a $Bi/Te(+Se+S)$ ratio equal to or slightly higher than 1 (Fig. 7) suggests more reduced conditions.

Hessite is the most abundant telluride in El Valle deposit, but alone is not a good mineral to provide information on ore-forming conditions because it is stable over a wide range of fO_2 conditions (*Zhang* and *Spry*, 1994). Calaverite, on the other hand, has a narrow stability field in terms of fO_2, which overlaps both the hematite-magnetite and pyrite-hematite buffers (*Zhang* and *Spry*, 1994). We can suppose similar conditions for the bornite-rich ore from calcic skarn. In addition, the abundance of clausthalite in these ore samples, and absence of galena, implies conditions of relatively high fSe_2/fS_2 and fO_2 (*Simon* et al., 1997).

The stability fields of some of studied minerals, in terms of fS_2 and fTe_2, are shown on Fig. 8, drawn for a temperature of 300 °C, which is considered a valid approximation of the formation temperature of the TSB minerals (see above). Those sulfides and oxides commonly present in the ores have also been included in this diagram. In both the El Valle and Ortosa deposits, the field of hessite stability

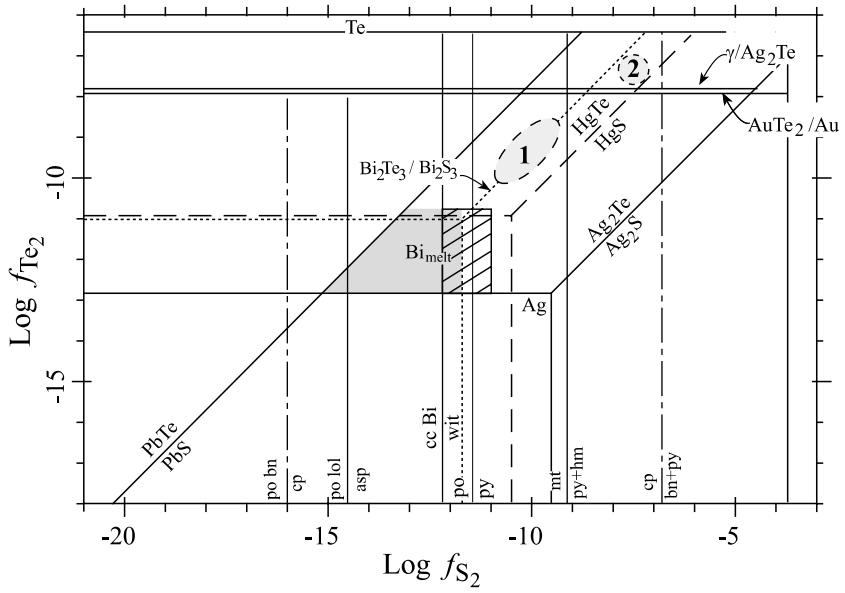

Fig. 8. Telluride–sulfide stability diagram at 300 °C in fTe_2–fS_2 space, after *Afifi* et al. (1988a, b), for the different gold assemblages: **a** medium gray area corresponds to Ortosa ores; **b** pattern area corresponds to magnesian skarn ores from El Valle; **c** domains marked '1' and '2' correspond to proximal and distal calcic skarn ores from El Valle, respectively (see text for details). Abbreviations: asp: arsenopyrite, bn: bornite, cc: chalcocite, cp: chalcopyrite, hm: hematite, lol: löllingite, mt: magnetite, po: pyrrhotite, py: pyrite, wit: wittichenite

with respect to Ag-rich electrum or argentite defines the minimum fS_2–fTe_2 conditions required for the stability of the other telluride minerals (*Afifi* et al., 1988a). In Fig. 8, this field has been calculated for electrum with minimum silver composition of $N_{Ag} = 0.5$ (*Afifi* et al., 1988a; *Barton* and *Toulmin*, 1964), indicating minimum conditions of $\log fTe_2$ of around -13. The upper limit of fTe_2 is constrained by the absence of PbTe and native tellurium.

At the El Valle deposit, the presence of wittichenite in the magnesian skarn ores constrains the values to more than $-12 \log fS_2$. Only locally is the fTe_2 sufficiently high to form Bi-tellurides (tsumoite and kawazulite). Moreover, the presence of coloradoite (HgTe) indicates $\log fTe_2$ values above the Hg–HgTe reaction. In the calcic skarn, the assemblage gold–tetradymite–bismuthinite indicates fTe_2/fS_2 ratios along the stability boundary between bismuthinite and tellurobismuthite (Fig. 8) and below the Au–$AuTe_2$ reaction. Another mineral present in this association is aikinite ($PbCuBiS_3$), but there is no thermodynamic data available for the Pb–Cu–Bi–S system.

In the bornite-rich calcic skarn, the gold assemblages consist of Au–Ag-tellurides, mainly hessite, petzite and sylvanite, with scarce calaverite. We have insufficient data to indicate if these precious metal tellurides were originally formed as an equilibrium assemblage or are a product of decomposition of χ and/or γ phases (*Cabri*, 1965). As mentioned above, Ag-rich sylvanite is to be expected where it forms in equilibrium with petzite (*Shackleton* et al., 2003). According to *Afifi* et al. (1988a), the lower fTe_2 limits for the stability of Au–Ag di-tellurides, petzite and sylvanite, correspond roughly to the hessite-γ reaction.

At the Ortosa deposit, the typical assemblage (native bismuth–gold–hedleyite–joséite-B) limits the conditions along the boundary Bi–Bi_2Te_3, within the pyrrhotite stability field. The PbTe–PbS reaction constrains the fTe_2 and fS_2 values due to the presence of galena and the absence of altaite. The occurrence of hessite, bismuthinite and joséite-A may indicate an increase in fS_2 as suggested by the replacement of pyrrhotite by pyrite.

The fields that represent the more likely conditions of formation for the different mineral assemblages studied have been drawn on Fig. 8. The mineral assemblages from Ortosa and El Valle magnesian skarn do not indicate an important increase of the fTe_2 values, although in the latter the conditions were at higher fO_2 and/or fS_2. In the case of El Valle calcic skarn, an increase in the fTe_2/fS_2 ratios from the proximal skarn to the wollastonite-bearing distal skarn is observed.

Conclusions

Our study on the gold-related tellurides, selenides and Bi-sulfosalts from two different types of skarn (Cu–Au skarn from the El Valle deposit and Au-skarn from the Ortosa deposit) may provide new data to help characterize these minerals as tracers of physicochemical conditions of ore formation. We can draw the following conclusions:

In the two skarns, different mechanisms lead to Au-enrichment in the ores. At the El Valle deposit, gold, along with Cu, was incorporated in a Ag–Bi-rich $bornite_{ss}$ at high temperatures. Prolonged cooling led to exsolution of the observed accessory minerals. The abundance of tellurides and selenides in the bornite-rich ore is a consequence of bornite being able to accommodate large amounts of trace elements at high temperatures. At the Ortosa deposit, gold, and probably also bismuth, were released during the transformation of löllingite to arsenopyrite. Apart from this, in both deposits, gold was remobilized from mineralizing fluids as Au($\pm$Ag)–Bi–Te($\pm$Se)–S_{ss} droplets and crystallized in equilibrium with the host minerals.

The TSB in El Valle skarn ores, with $Bi/Te(+Se+S) \leq 1$, are consistent with the stability of magnetite. The presence of tetradymite and kawazulite with $Bi/Te(+Se+S) < 1$, or tsumoite with $Bi/Te(+Se+S) \approx 1$, may indicate minor variations in the redox conditions. In the bornite-rich calcic skarn, the abundance of clausthalite and Au–Ag di-tellurides is explained by higher oxidation conditions that overlap the pyrite-hematite buffer, in addition to higher fTe_2/fS_2 and fSe_2/fS_2 ratios.

In contrast, the TSB found in ores form the Ortosa deposit (hedleyite, joséite-B, -A, laitakarite-ikunolite) have a $Bi/Te(+Se+S)$ ratio ≥ 1, corresponding to more reduced conditions within the pyrrhotite stability field, which is consistent with the petrographic observations.

Acknowledgements

We express our gratitude to Río Narcea Gold Mines for financial support and for data provided. This work has also been financed by CICYT project number MCT01BTE3469 (Science and Technology Ministry of Spain). We thank *Nigel J. Cook* and two other anonymous reviewers, as well as Guest Editor *Cristiana L. Ciobanu*, for their constructive comments and suggestions that greatly improved this manuscript.

References

Afifi AM, Kelly WC, Essene EJ (1988a) Phase relations among tellurides, sulfides, and oxides: I. Thermochemical data and calculated equilibria. Econ Geol 83: 377–394

Afifi AM, Kelly WC, Essene EJ (1988b) Phase relations among tellurides, sulfides, and oxides: II. Applications to telluride-bearing ore deposits. Econ Geol 83: 395–404

Arcos D (1996) Las mineralizaciones asociadas a la granodiorita en el depósito de Cu–Au de Carlés (Asturias). Unpub Thesis, University of Barcelona

Arcos D, Soler A, Delgado J (1995) Fluid evolution in the Cu–Au deposit related to the Carlés Granodiorite (Asturias). Eur J Mineral 8: 975–985

Barton PB Jr, Skinner BJ (1979) Sulfide mineral stabilities. In: *Barnes HL* (ed) Geochemistry of hydrothermal ore deposits. Wiley Intersci, New York, pp 278–403

Barton PB Jr, Toulmin P (1964) The electrum-tarnish method for determination of the fugacity of sulphur in laboratory sulphide systems. Geochim Cosmochim Acta 28: 619–640

Berman RG (1991) Thermobarometry using multiequilibrium calculations: a new technique with petrologic applications. Can Mineral 29: 833–855

Burt DM (1971) Multisystems analysis of the relative stabilities of babingtonite and ilvaite. Carnegie Inst Wash Year Book 70: 189–197

Cabri LJ (1965) Phase relations in the Au–Ag–Te system and their mineralogical significance. Econ Geol 60: 1569–1606

Campa D, Fuertes-Fuente M, Martín-Izard A (2001) Fluid inclusions in the Ortosa Au-skarn, Asturias (Northwester of Spain). XVI ECROFI. Extended abstract volume. Memórias do Departamento de Geologia do Porto 7: 49–52

Cathelineau M (1988) Cation site occupancy in chlorites and illites as a function of temperature. Clay Minerals 23: 471–485

Cepedal A (2001) Geología, mineralogía evolución y modelo genético del yacimiento de Au–Cu de ''El Valle-Boinás'', Belmonte (Asturias). Unpub Thesis, University of Oviedo

Cepedal A, Martín-Izard A, Reguilón R, Rodríguez-Pevida L, Spiering E, González-Nistal S (2000) Origin and evolution of the calcic and magnesian skarns hosting the El Valle-Boinás copper–gold deposit, Asturias (Spain). J Geochem Explor 71: 119–151

Cepedal A, Moreiras D, Martín-Izard A, González-Nistal S, Rodríguez-Pevida L (2003) The occurrence and origin of babingtonite in the El Valle-Boinás Cu–Au deposit in Asturias, Spain. Eur J Mineral 15: 1069–1077

Ciobanu CL, Cook NJ (2002) Tellurides, selenides (and Bi-sulphosalts) in gold deposits. 11th Quadrennial IAGOD symposium-Geocongress 2002, Windhoek, Namibia, July 2002. CD volume of extended abstracts. Geological Survey of Namibia

Ciobanu CL, Cook NJ, Pring A (2005) Bismuth tellurides as gold scavengers. In: *Mao JW, Bierlein FP* (eds), Mineral deposit research: meeting the global challenge, Springer, Berlin-Heidelberg-New York, pp 1383–1386

Ciobanu CL, Cook NJ, Damian G, Damian F (2006) Gold scavenged by bismuth melts: An example from Alpine shear-remobilizates in Highiş, Romania. Mineral Petrol (this volume)

Cook NJ, Ciobanu CL (2001) Paragenesis of Cu–Fe ores from Ocna de Fier-Dognecea (Romania), typifying fluid plume mineralisation in a proximal skarn setting. Mineral Mag 65: 351–372

Cook NJ, Ciobanu CL (2003) Lamellar minerals of the cuprobismutite series and related paděraite: a new occurrence and implications. Mineral Mag 41: 441–456

Cook NJ, Ciobanu CL (2004) Bismuth tellurides and sulphosalts from Larga hydrothermal system, Metaliferi Mts, Romania: Paragenesis and genetic significance. Mineral Mag 68: 301–321

Corretgé G, Suárez O (1990) Igneous rocks. In: *Dallmeyer RD, Martínez-Gracía E* (eds), Pre-Mesozoic geology of Iberia. Springer-Verlag, Berlin, pp 72–80

Dobosi G, Nagy B (1989) The occurrence of an Au–Bi sulphide in the Nagybörzöny hydrothermal ore deposit, Northern Hungary. N Jahrb Mineral Monatsh: 8–14

Douglas N, Mavrogenes J, Hack A, England R (2000) The liquid bismuth collector model: an alternative gold deposition mechanism. AGC Abstr 59: 135

Fuertes-Fuente M, Martín-Izard A, García-Nieto J, Maldonado C, Varela A (2000) Preliminary mineralogical and petrological study of the Ortosa Au–Bi–Te ore deposit: a reduced gold skarn in the northern part of the Río Narcea Gold Belt, Asturias, Spain. J Geochem Explor 71: 177–190

Fuertes-Fuente M, Cepedal A, Martín-Izard A, González-Nistal S, Barrero M (2004) The low temperature hydrothermal Au-mineralization in the El Valle deposit, Spain: A Carlin type deposit in the Río Narcea Gold Belt. 32 International Geological Congress, Florence. Program and Abstract CD-ROM

García Iglesias J, Loredo J (1990) Geological, mineralogical and geochemical characteristics of the Carlés gold mineralization, Asturias, Spain. Mineral Deposita 25 [Suppl]: 53–58

Gutiérrez Claverol M, Luque C, Martínez García E, Luque C, Suárez V, Ruíz F (1991) Gold deposits, late Hercynian tectonics and magmatism in the northeastern Iberian Massif (NW Spain). Chron Rech Min 503: 3–13

Jahoda C, Andrews J, Foster R (1989) Structural controls of Monte Roso and other gold deposits in NW Spain, fractures jogs and hot-jogs. Trans Inst Min Metall B 98: 1–6

Jambor JL, Puziewicz J (1990) New mineral names. Am Mineral 75: 1209–1216

Johnson JW, Norton D (1985) Theoretical prediction of hydrothermal conditions and chemical equilibria during skarn formation in porphyry copper systems. Econ Geol 80: 1797–1823

Kesler SE, Chryssoulis SL, Simon G (2002) Gold in porphyry copper deposits: its abundance and fate. Ore Geol Rev 21: 103–124

Kretschmar U, Scott SD (1976) Phase relations involving arsenopyrite in the system Fe–As–S and their application. Can Mineral 14: 364–386

Martín-Izard A, Boixet Ll, Maldonado C (1993) Geology and mineralogy of the Carlés copper–gold-bearing skarn, Cantabrian Cordillera, Spain. In: *Fenoll Hach-Ali P, Torres-Ruiz J, Gervilla F* (eds), Current research in geology applied to ore deposit, Univ Granada, pp 499–502

Martín-Izard A, Fuertes-Fuente M, Cepedal A, Moreiras D, García-Nieto J, Maldonado C, Pevida LR (2000a) The Río Narcea Gold Belt intrusions: geology, petrology, geochemistry and timing. J Geochem Explor 71: 103–117

Martín-Izard A, Paniagua A, García-Iglesias J, Fuertes-Fuente M, Boixet Ll, Maldonado C, Varela A (2000b) The Carlés copper–gold-molybdenum skarn (Asturias, Spain): geometry, mineral associations and metasomatic evolution. J Geochem Explor 71: 153–175

McQueen KG, Larson RA (1985) The occurrence of wittichenite and sulphide exsolution textures at the Glen deposit, Wee Jasper, New South Wales. N Jahrb Mineral Monatsh 10: 469–480

Meinert LD (2000) Gold in skarns related to epizonal intrusions. Rev Econ Geol 13: 347–375

Oen IS, Kieft C (1976) Silver-bearing wittichenite-chalcopyrite–bornite intergrowths and associated minerals in the Mangualde pegmatite, Portugal. Can Mineral 14: 185–193

Oen IS, Kieft C (1984) Paragenetic relations of Bi-, Ag-, Au- and other tellurides in bornite veins at Glava, Värmland, Sweden. N Jahrb Mineral Abh 149: 245–266

Paar WH, Putz H, Roberts AC, Stanley CJ, Culetto FJ (2006) Jonassonite, $Au(Bi,Pb)_5S_4$, a new mineral species from Nagybörzsöny, Hungary. Can Mineral (in press)

Pérez Estaún A, Bastida F (1990) Cantabrian and Palentian Zones: Structure of the Cantabrian Zone. In: ■ *RD, Martínez-García E* (eds) Pre-Mesozoic geology of Iberia. Dallmeyer Springer-Verlag, Berlin, pp 55–69

Shackleton JM, Spry PG, Bateman R (2003) Telluride mineralogy of the Golden Mile deposit, Kalgoorlie. Can Mineral 41: 1503–1524

Sharp ZD, Essene EJ, Kelly WC (1985) A reexamination of the arsenopyrite geothermometer: pressure considerations and applications to natural assemblages. Can Mineral 23: 517–534

Shvedenkov GYu, Mazurov MP (1977) Stability of babingtonite in the system Ca–Fe–Si–O–H. Trans USSR Acad Sci, Earth Sci 232: 178–181

Simon G, Kesler SE, Essene EJ (1997) Phase relations among selenides, sulfides, tellurides and oxides: II applications to selenide-bearing ore deposit. Econ Geol 92: 468–484

Simon G, Kesler SE, Essene EJ, Chryssoulis SL (2000) Gold in porphyry copper deposits: experimental determination of the distribution of gold in the Cu–Fe–S system at 400° to 700 °C. Econ Geol 95: 259–270

Spiering ED, Pevida LR, Maldonado C, González S, García J, Varela A, Arias D, Martín-Izard A (2000) The gold belts of western Asturias and Galicia (NW Spain). J Geochem Explor 71: 89–101

Tomkins AG, Mavrogenes JA (2001) Redistribution of gold within arsenopyrite and löllingite during pro- and retrograde metamorphism: application to timing of mineralization. Econ Geol 96: 525–534

Walshe JL (1986) A six-component chlorite solid solution model and the conditions of chlorite formation in hydrothermal and geothermal systems. Econ Geol 81: 681–703

Zhang X, Spry PG (1994) Calculated stability of aqueous tellurium species, calaverite, and hessite at elevated temperatures. Econ Geol 89: 1152–1166

Authors' addresses: *A. Cepedal* (corresponding author; e-mail: mcepedal@geol.uniovi.es), *M. Fuertes-Fuente* and *A. Martín-Izard*, Department of Geology, University of Oviedo, C/Arias de Velasco s/n, 33005, Asturias, Spain; *S. González-Nistal* and *L. Rodríguez-Pevida*, Río Narcea Gold Mines, Avda. Del Llaniello 13, 33860 salas, Asturias, Spain

Dear Author,

The goal of our new, more rapid publication procedures is to publish your paper online as quickly as possible. The assigning of a DOI (digital object identifier) at this stage means that the work is fully citeable much earlier than has previously been the case. Please note that final pagination will be added only when articles have been assigned to a printed issue. With respect to the quality of figures in the electronic version, please note that the printed version will be of the usual high quality. For a list of all papers published online so far, please refer to the following web-site (your paper will be added to this list after final correction):

http://link.springer.de/link/service/journals/00710/tocs.htm

Offprint Order

Journal: Mineralogy and Petrology MS No.: 0/127 First Author: A. Cepedal

50 Offprints of each paper are supplied **free of cost;** the order of additional offprints against payment must be sent in when returning the corrected proofs.
The prices quoted are valid only for authors ordering offprints for their private use.
Please write clearly in capital letters!

NEW **When you order offprints against payment, you are entitled to receive in addition a pdf file of your article for your own personal use.** As this pdf file is sent to you by e-mail, please insert the e-mail address here: _____

In addition of the free offprints, I hereby order against payment

☐ **50** ☐ **100** ☐ **200** ☐ **300** ☐ **400** **offprints**

Offprints should be sent to:

_____
(Name of person or institution)

_____
(Address)

_____

Payment will be made by:

_____
(Name of person or institution)

_____
(Address)

_____

(Purchase Order No.) _____ (Date/Signature of author) _____

☐ Please bill me **(please do not pay for offprints before receipt of invoice!)**

☐ Please charge my credit card ☐ Eurocard / Mastercard ☐ American Express
☐ Visa ☐ Diners Club

No.: | | | | | | | | | | | | | | | | Valid until: | | / | |

Signature: _____

(In all separate correspondence concerning this order please quote the Journal's title, MS No., and First Author.)

Price list for offprints* Prices include carriage charges (surface mail). Prices are subject to change without notice.

***Customers in foreign EU countries:** Please state your V.A.T. registration number if applicable. Otherwise we have to add 10% V.A.T. to the list prices.

V.A.T. registration number: _____

Pages (Figs. incl./excl.)	50 Copies	100 Copies	200 Copies	300 Copies	400 Copies
	EUR	EUR	EUR	EUR	EUR
☐ 1–8	296,–	348,–	482,–	598,–	722,–
☐ 9–16	384,–	436,–	626,–	806,–	998,–
☐ 17–24	462,–	512,–	742,–	972,–	1198,–
☐ 25–32	512,–	564,–	844,–	1098,–	1408,–

Please return your order form to:
Springer Wien New York, Production Department, **Sachsenplatz 4-6, P.O. Box 89, 1201 Wien, Austria**

Copyright Transfer Statement

The copyright to this article is hereby transferred to Springer (for US Government employees: to the extent transferable), effective if and when the article is accepted for publication. The copyright transfer covers the exclusive rights to reproduce and distribute the article, including reprints, photographic reproductions, microform, electronic database, videodiscs, or any other reproductions of similar nature, and translations.
However, the authors reserve:
1. All proprietary rights other than copyrights, such as patent rights.
2. The right to use all or part of this article in future works of their own and to grant or refuse permission to third parties to republish all or part of the article or translations thereof. To republish whole articles, such third parties must obtain written permission from Springer as well. However, Springer may grant rights concerning journal issues as a whole.

To be signed by at least one of the authors who agrees to inform the others, if any.

_____
(Author's signature)

Instruction to printer	Mark	Examples	
		In the text	In the margin
Character to be corrected		Letter to be corrected	e /
Group of characters to be corrected		Letters to be corrected	ed H
Several identical characters to be corrected		Council or Commission	o ///
Differentiation of several errors in the same paragraph	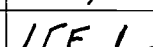	There are many faults in this lane	r/ m/ aF i L i J
Character or word to be deleted		Commission and and Parliament	y y H
Character or word to be added		A word missing	is λ
Superior character required		The Court's judgment.	(1) /
Omitted text to be added (see copy)		1. January 12. December	Out see copy
Inferior character required		H_2SO_4	4 /
Change to italic		Ad infinitum	ital.
Change italic characters to roman		*status quo*	rom.
Change capitals to lower case		UNESCO	l.c.
Change to capitals or small capitals		Robert burns, AD 1759-96	caps. s.c.
Change to bold face		This word needs emphasising!	bold
To be letter-spaced		These letters need space	/
Correct horizontal alignment		This line is crooked	/
Text to be raised or lowered		This is a line uneven	/ /
Text to be aligned (to the left)		This text is to be aligned	/
Text to be aligned (to the right)		This text is to be aligned	/
Text to be centred		This text is to be centred	/
Take back to previous line		This hyph- en is unnecessary	/
Text to run on (no new paragraph)		... line. No new paragraph here	/
Take forward to next line		This hy- hen is badly placed	/
Create new paragraph		... line. A new paragraph should begin here	/
Close up		A space is wrong here	/
Equalise space		This spacing is very uneven	/
Add space between words		A space is missing here	# /
Reduce space between words		These spaces are too big!	/
Add space between lines		These lines are too close together	#
Reduce space between lines		These lines are too far apart.	/
Stet (let original text stand)		This text was corrected error	✓
Transpose characters		These letters are transposed	/
Transpose words		These are words transposed	/
Transpose lines		transposed These lines are	/

NB: A correction made in the text must always have a corresponding mark in the margin, otherwise it may be overlooked when the corrections are made. The same marks should be used, where appropriate, by copy-editors marking up copy. Where instructional words are used in marginal marks, e.g. 'ital.', 'bold', etc., they must always be encircled to show that they are not to be printed.

33,3% cheaper for you . . .

As an author of Springer Wien New York you are now entitled to receive a 33,3% price reduction on the list price of all books published by the Springer group. For your order please use this order form. Orders have to be sent directly to Springer Wien New York.

Als Autor/in von Springer Wien New York erhalten Sie 33,3% Rabatt auf den Ladenpreis der **gesamten Buchproduktion** der Springer-Gruppe. Bitte bestellen Sie mit diesem Bestellschien. Ihre Bestellung senden Sie bitte ausschließlich an Springer Wien New York.

For detailed informations about titles published by Springer Wien New York please search our homepage.
Nähere Informationen über das Programm von Springer Wien New York finden Sie auf unserer Homepage. **www.springer.at**

Order Form/Bestellschein

Springer Wien New York, Order Department, Sachsenplatz 4–6, P. O. Box 89, 1201 Wien, Austria, Fax +43-1-330 24 26
Springer Wien New York, Auslieferung, Sachsenplatz 4–6, Postfach 89, 1201 Wien, Österreich, Fax +43-1-330 24 26

I order herewith/Ich bestelle hiermit:

copy/ies	ISBN	Author	Title
Expl.	ISBN	Autor	Titel

Please copy this order form for your next orders. Bitte kopieren Sie diesen Bestellschein fur Ihre weiteren Bestellungen.

○ Please bill me/Bitte liefern Sie gegen Rechnung

○ Please charge my credit card/Bitte belasten Sie meine Kreditkarte

○ VISA ○ MASTERCARD ○ AMEX ○ DINERS

Card No./Karten-Nr. _____ Expiry date/Gültig bis_____

NAME/NAME _____

ADDRESS/ADRESSE _____

_____

DATE/DATUM _____

SIGNATURE/UNTERSCHRIFT _____